

EFFECT OF THERMAL AND WELD-  
INDUCED RESIDUAL STRESSES ON  
THE J-INTEGRAL AND CTOD IN  
ELASTIC-PLASTIC FRACTURE  
ANALYSES

P. Delfin, I. Sattari-Far and B. Brickstad

Final Report

SINTAP/SAQ/03

June 1998

**SAQ KONTROLL AB**

Box 49306

SE-100 29 Stockholm

SWEDEN

ABSTRACT .....	2
1. INTRODUCTION.....	3
2. SIMULATION OF THE WELDING PROCESS AND CRACK GROWTH.....	4
2.1 The finite element model.....	4
2.2 Thermal analysis.....	6
2.3 Structural analysis.....	7
2.4 Simulation of crack growth.....	9
3. A WELDED PIPE SUBJECTED TO A PRIMARY LOAD.....	9
3.1 The contribution from residual stresses to $J$ and $CTOD$ during axial loading.....	9
3.2 Relaxation of residual stresses due to unloading.....	16
3.3 Different tangent modulus.....	16
3.4 The effect of using linear isotropic hardening in the calculation of $J$ and $CTOD$ .....	22
4. A WELDED PIPE SUBJECTED TO A THERMAL LOAD.....	24
5. DISCUSSION.....	28
6. CONCLUSIONS.....	29
REFERENCES.....	31
APPENDIX A. EPRI/GE 'S TREATMENT OF THERMAL STRESSES.....	33
APPENDIX B. THE $J$ -INTEGRAL AND THE $CTOD$ AS FRACTURE PARAMETERS.....	38
APPENDIX C. CTOD EVALUATION IN POWER LAW MATERIALS.....	43
APPENDIX D. A HANDBOOK-BASED LIMIT LOAD DEFINITION.....	45

**ABSTRACT**

An investigation of how the residual stress of a welded pipe contributes to the *CTOD* and the *J*-integral has been performed. Many experiments show that for ductile materials and high  $L_r$  values the contribution from the residual stress to the risk of fracture is negligible. The objective of the present numerical analyses is to investigate how the weld residual stresses interact with other types of stresses and if possible give some recommendations on how to treat weld residual stresses in fracture assessments. The welding process has been simulated according to generally accepted methods in order to obtain a proper plastic strain field. The results imply that although the relative contribution of the residual stress to fracture decreases rapidly for high  $L_r$ , the residual stresses still make a non-negligible contribution even for quite high loads.

## 1. INTRODUCTION

Structures may fail because of crack growth both in welds and in the heat affected zone (HAZ). The welding process itself induces residual stresses in the weld and HAZ, which contribute to crack growth. The mechanism of growth can be sub critical i.e. IGSCC or fatigue, or critical growth initiation. Several references regarding simulation of the welding process can be found in a recent report on welding in stainless steel pipes by Brickstad and Josefson [1], and also in Hou et al. [2]. Two examples of studies on crack growth in welds are [2] and Kanninen et al. [3]. It is not self evident which characterising fracture parameter to use when the crack is subjected to weld-induced stresses. This study as well as others, e.g. [2] demonstrates the difficulties using the  $J$ -Integral. Crack opening measures are often proposed, e.g. in [2] and [3]. In this report both the  $J$ -Integral and the  $CTOD$  (Crack Tip Opening Displacement), obtained by the  $90^\circ$ -interception construction, are calculated, and their validity and usefulness are discussed.

The main purpose of this work is to investigate the significance of the residual stresses for cracks in ductile materials with nuclear applications. The treatment of weld-induced stresses as expressed in the handbook by Andersson et al [4] is believed to be conservative for ductile materials. This is because of the general approach not to account for the improved fracture resistance caused by ductile tearing and furthermore there is experimental evidence that the contribution of residual stresses to fracture diminishes as the degree of yielding increases to a high level. Green et al [5,6] and Sharples et al [7-9] showed in a series of experiments that at low levels of yielding, i.e. small  $L_r$ , the influence of the residual stresses was large, but near plastic instability ( $L_r = 1$ ) weld-induced stresses were of little importance. Available procedures for flaw assessments, such as the ASME XI code [10] and the R6 procedure [11] treat this issue differently. For instance, the ASME XI code does not consider weld-induced residual stresses in some materials e.g. stainless steel welds. Neglecting weld-induced stresses in general, though, is doubtful for loads that are mostly secondary (e.g. thermal shocks) and for materials which are not ductile enough to be limit load controlled.

In order to demonstrate the effect of weld-induced residual stresses on  $J$  and  $CTOD$ , a series of analyses have been performed. A non-linear thermoplastic finite element model was adopted to simulate the circumferential weld in a relatively thin-walled stainless steel pipe. A commercially available FEM code, ABAQUS [12], was used for the calculations. After the pipe had cooled down after welding a circumferential surface crack was introduced. The crack, located in the centre of the weld, was subjected to two types of loads. Firstly, the welded pipe was subjected to a primary tensile load, and then to a secondary thermal load. The  $J$ -integral and the  $CTOD$  were calculated during the complete histories of the tensile and thermal load. These results were compared with results from equivalent analyses but with no residual stresses present. This made it possible to

qualitatively obtain some understanding on how the contribution of the residual stresses to fracture is affected by the magnitudes of the primary and secondary loads.

## 2. SIMULATION OF THE WELDING PROCESS AND CRACK GROWTH

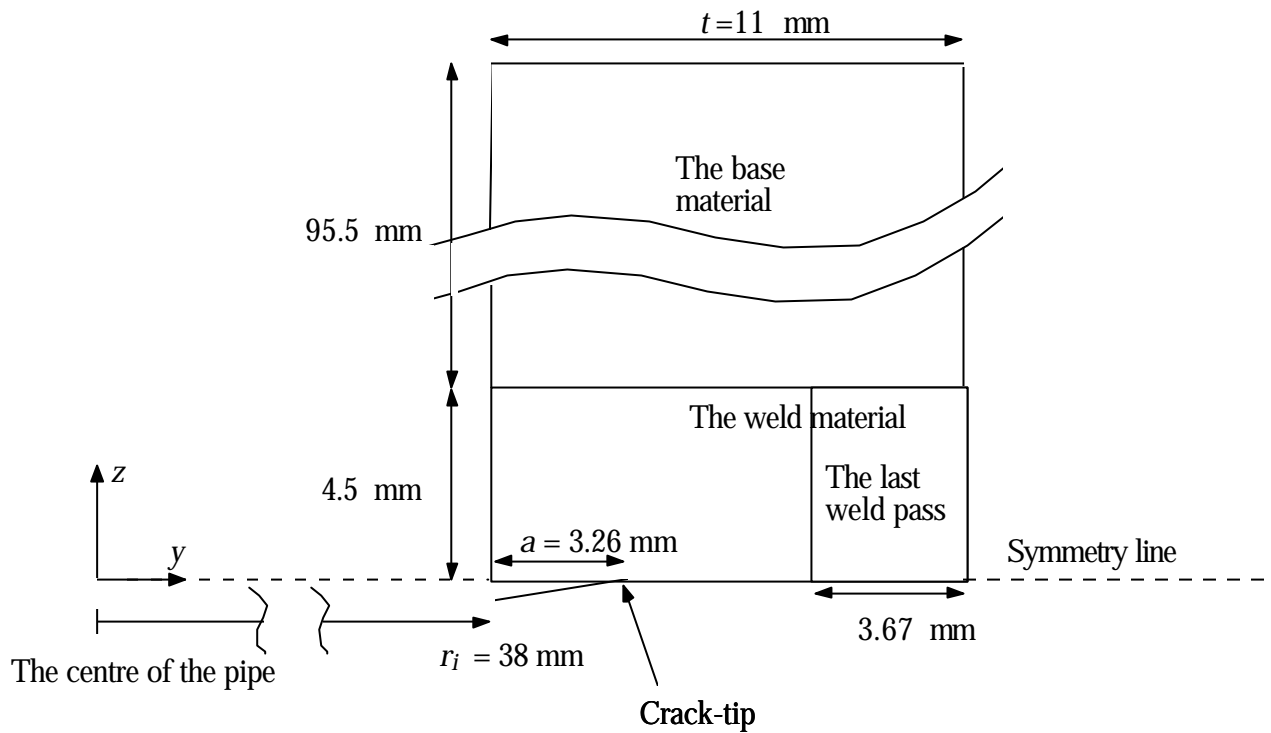
The modelled pipe has an inner radius,  $r_i = 38$  mm and a wall-thickness,  $t = 11$  mm. The geometry is depicted in figure 1. The weld is oriented circumferentially. The choice of geometry is guided by the type of stress field obtained for thin walled pipes. The axial stresses are essentially through-thickness bending whereas in a thick-walled pipe they are more complex and also less severe. A non-linear uncoupled thermoplastic based model was used. The thermal analysis and the stress analysis are described in the two following subsections. The general procedure of simulation follows that of Brickstad and Josefson [1].

The geometry of the weld modelling are simplified in the following ways.

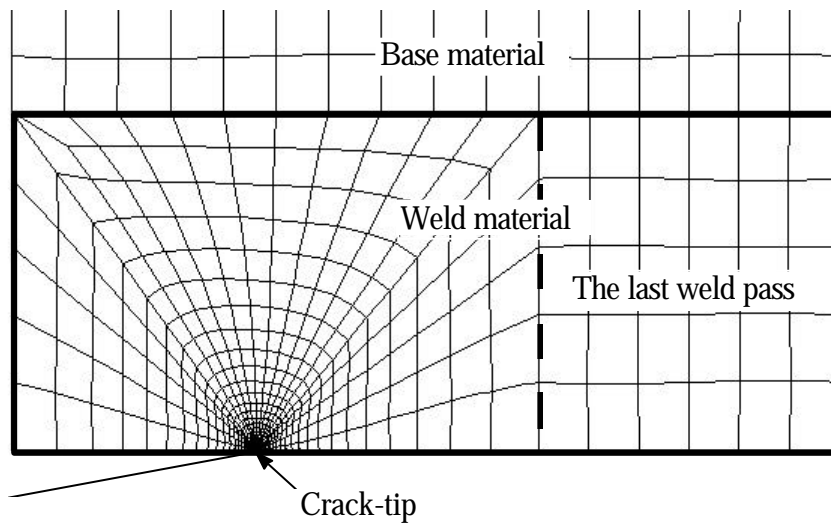
- Only the last weld pass is modelled. This is motivated by the fact that for a thin-walled pipe such as in this case, the last pass in a series of passes will cause a uniform heating of the entire thickness of the pipe.
- Only half the pipe section is modelled because the crack plane coincides with the symmetry plane.
- It has been observed that the residual stresses in a circumferentially welded thin-walled pipe are approximately rotationally symmetric. This justifies the use of an axisymmetric model.
- The weld geometry is somewhat simplified, a rectangular groove has been used.

### 2.1 The finite element model

The same mesh has been used in both the thermal and the stress analysis. The elements used are eight-noded biquadratic axisymmetric with full integration, which have proved to give the best convergent behaviour. The crack plane is also the symmetry plane which allows for the modelling of only half the pipe section, see figure 1a-b). Anticipating that a crack is to be introduced the mesh is focused on a point where the crack-tip will be located. The smallest elements used are small ( $\approx 10^{-3}$  mm). This was necessary in order to evaluate the *CTOD* at low load levels. In Appendix C a separate study is presented in order to determine a suitable finite element model. The FEM code ABAQUS [12] uses a Newton iteration method improved by a line search algorithm, which is effective when the initial iterations are relatively far from the solution.



a)



b)

**Figure 1.** a) The geometry of a cross section of the pipe wall in the  $z$ -direction. Only half the pipe is shown due to symmetry.  
b) Detail of the mesh used in the finite element analysis.

## 2.2 Thermal analysis

The thermal problem was treated as follows: An heat flux [ $\text{W}/\text{m}^3$ ] was activated in the weld material that constitutes the last pass. The use of only the last weld pass simplifies the calculations substantially in the respect that birth of elements need not be considered. An unrealistic consequence of the assumption of axial symmetry is that the heat flux is applied instantaneously around the circumference of the pipe. This can to some extent be compensated for by assuming that the heat flux is applied during a finite period in time with an assumed triangular time variation corresponding to the approach and passing of the weld torch. The heat flux  $h$  can be expressed as

$$h = \frac{v}{V_p} Q_{line} , \quad (1)$$

where  $Q_{line}$  is the net line energy [ $\text{J}/\text{m}$ ] used during the welding and  $v$  is the travel speed of the weld electrode,  $V_p$  is the weld pass volume. However the weld pass volume  $V_p$  can not be defined in a 2-D model and must be chosen in such a way that some empirical observations are satisfied. The molten zone size and the distance from the weld-base material interface to HAZ must be realistic [1]. Once its value has been set the duration  $Dt$  of the heat flux period can be determined from

$$Dt = \frac{V_p}{A_p v} \quad (2)$$

where  $A_p$  is the area of the cross section of the weld pass. However it should be pointed out that the objective here is to achieve relatively high residual stress levels and properly infer the residual stresses through plastic strains, rather than simulating a particular stress field.

The boundary conditions allow for both convection and radiation. The axisymmetric conditions assumed mean that heat losses in the axial direction are neglected. Radiation losses are dominant for higher temperatures near the weld. Convection losses are important for lower temperatures some distance away from the weld. A combined boundary condition, which takes into account both radiation and convection is used in this work, Argyris et al [13]. The resulting heat transfer coefficient  $\alpha_h$  is

$$\begin{aligned} \mathbf{a}_h &= 0.0668 \cdot T \text{ W}/\text{m}^2, & 0^\circ\text{C} < T < 500^\circ\text{C} \\ \mathbf{a}_h &= 0.231 \cdot T - 82.1 \text{ W}/\text{m}^2, & T > 500^\circ\text{C} \end{aligned} \quad (3)$$

The other necessary thermal data for both the weld material and the base material are stated in the table below.

**Table 1**

<b>T</b> [°C]	<b>c<sub>p</sub></b> [J/kg°C]	<b>l</b> [W/m°C]	<b>a</b> [10 <sup>-6</sup> /°C]
20	442	15.0	19
200	515	17.5	19
400	563	20.0	19
600	581	22.5	19
800	609	25.5	19
1000	631	28.3	19
1200	654	31.1	19
1340	669	33.1	19
1390	675	66.2	19
2000	675	66.2	19

### 2.3 Structural analysis

In the structural analysis the temperatures taken from the thermal analysis are used to calculate the stresses. Only small strain theory is considered. In [1] it was observed that the difference in the weld-induced stresses between small strain theory and large strain theory is small. The von Mises yield criterion and associated flow rule are used together with kinematic hardening and a bilinear representation of the stress strain curve. Kinematic hardening rather than isotropic hardening is chosen because it is believed to better model reverse plasticity and the Bauschinger effect that is expected to occur during welding. It is also believed that an insufficient number of stress cycles occurs during the single-pass welding for symmetrization of the hysteresis loop to occur, a situation which would have been better represented by isotropic hardening. Nevertheless, the effect of using isotropic hardening has also been studied. The results are presented separately (Section 3.3). The use of only the last weld pass simplifies the calculations in the same way as in the thermal analysis in the respect that birth of elements need not be considered. The material in both the weld and the base have the same mechanical properties. This choice serves the purpose of limiting the number of parameters affecting the fracture problem. The mechanical material data are presented in Table 2.

**Table 2**

<b>T</b> [°C]	<b>E</b> [10 <sup>11</sup> Pa]	<b>n</b>	<b>s<sub>y</sub> base</b> [MPa]	<b>E<sub>T</sub>/E</b>
20	2.0	0.278	230	0.014
200	1.85	0.288	184	0.014
400	1.70	0.298	132	0.014
600	1.53	0.313	105	0.014
800	1.35	0.327	77	0.014
1000	0.96	0.342	50	1 · 10 <sup>-4</sup>
1200	0.50	0.350	10	1 · 10 <sup>-4</sup>
1340	0.10	0.351	10	1 · 10 <sup>-4</sup>
1390	0.10	0.353	10	1 · 10 <sup>-4</sup>
2000	0.10	0.357	10	1 · 10 <sup>-4</sup>

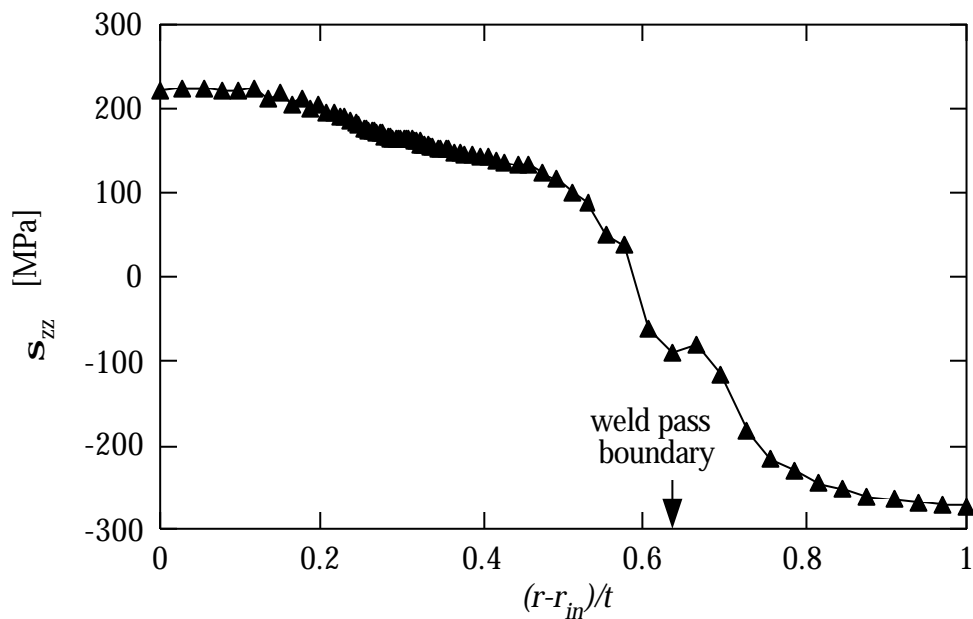


**Figure 2** The axial residual stress along the symmetry line i.e. in the weld centre line.

The resulting axial stress across the symmetry line at  $T = 22.5$  °C is shown in figure 2. For this relatively thin-walled pipe the stress distribution is mainly that of bending. The small bump at the weld pass boundary is believed to be a consequence of the numerical modelling. The crack will be introduced with its crack-tip located at 3.26 mm from the inside surface which is not close to the bump. Thus, the bump will not be of any significance for the fracture analysis.

## 2.4 Simulation of crack growth

After the welding process is over and the pipe has cooled down to room temperature a crack is introduced in the weld centre line by means of gradual node relaxation starting from the inside of the pipe. The final crack length is  $a = 3.26$  mm. The axisymmetry of the problem allows only for a completely circumferential crack to be modelled. The crack is restricted to grow in the radial direction. A physical growth mechanism can be stress corrosion or fatigue. The chosen method of sequentially releasing the nodes along the chosen growth direction gives a path dependent  $J$ -integral. This is simply because growth does not represent proportional loading. When the crack reached its final length, loads will be applied and as the loads are increased the  $J$ -integral becomes, from a practical view, path independent.

## 3. A WELDED PIPE SUBJECTED TO A PRIMARY LOAD

### 3.1 The contribution from residual stresses to $J$ and $CTOD$ during axial loading

An axial tensile load was applied to the pipe both with and without residual stress present. As the axial load, which is a primary load, was increased in very small steps the  $J$ -integral and the  $CTOD$  were calculated. The limit load parameter  $L_r$  is defined as  $P/P_g$  where  $P$  is the applied load and  $P_g$  is the limit load. For  $P = P_g$  the ligament is deformed plastically. In figure 3 the load-displacement curve  $P - d$  is presented and  $P_g$  is determined by the intersection of the two straight lines shown. The displacement,  $d$ , is evaluated at the loading point. The value of the limit load is found to be  $P_g = 228$  MPa. In this way it is possible to define a limit load from the finite element solution which in a sense is more physically motivated than for example handbook solutions, where the material is assumed to behave elastic perfectly-plastic. This  $L_r$ -solution is used throughout this paper. The solution obtained from the handbook [4], which assumes that the material behave elastic perfectly-plastically, gives  $P_g = 162$  MPa. The difference between these two definitions of  $P_g$  is quite significant. This can be explained by the effect of hardening and by the way the von Mises criterion is fulfilled. The introduction of a crack makes it possible for the stress components to redistribute in such way that the axial stress becomes greater than the yield stress in the ligament, which is not allowed for in the handbook solution [4]. To demonstrate the effect of this stress redistribution, the  $P - d$  curve for the considered material with vanishing hardening, is also shown in figure 3. The elastic perfectly-plastic limit load is then found to be 192 MPa.

Our definition of  $P_g$  is somewhat arbitrary. Other limit load solutions may be used and our results may then be calibrated accordingly by multiplying the  $L_r$  scales in figures 4-9 by an appropriate factor.

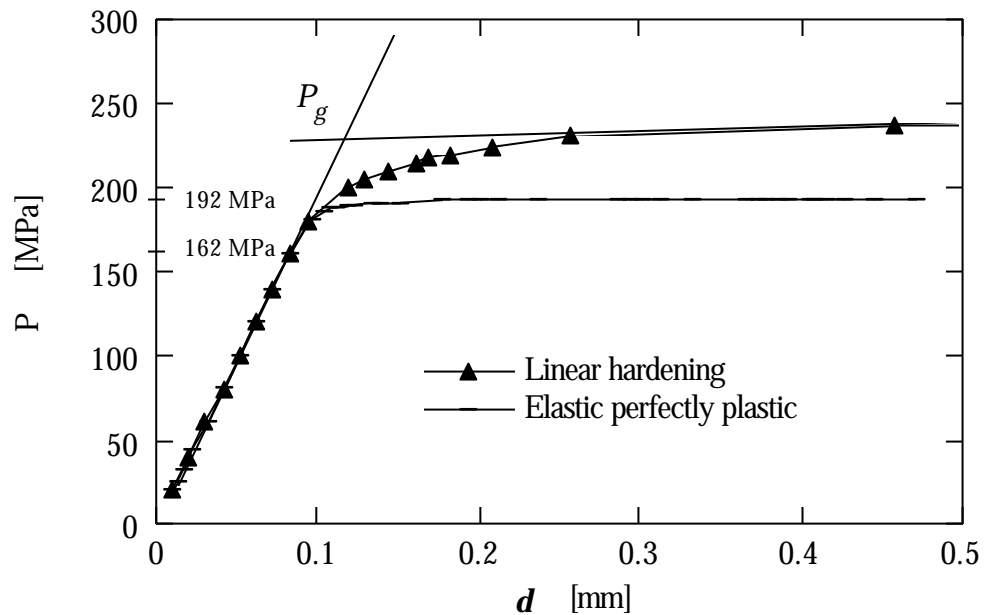
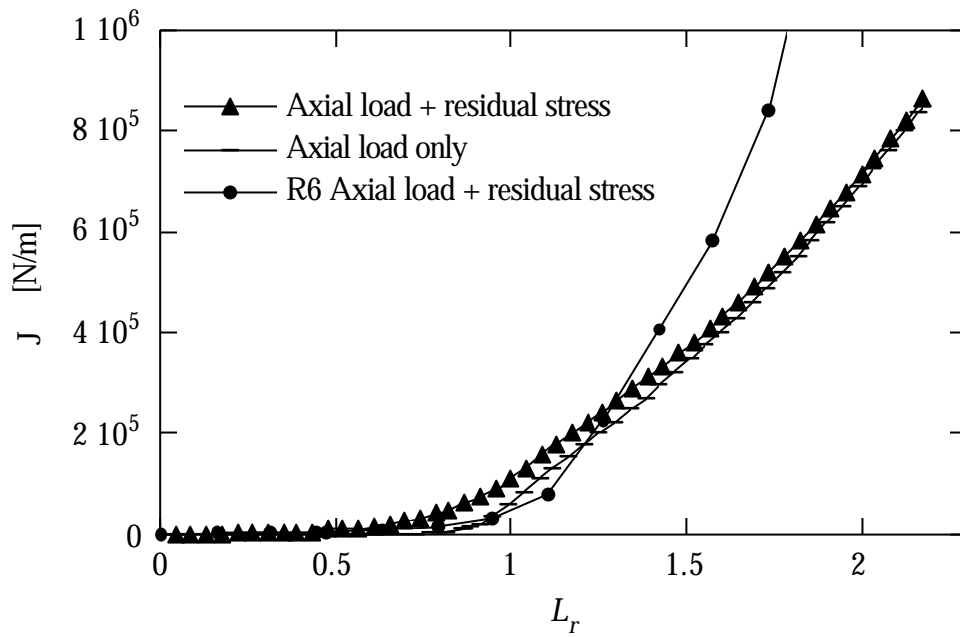
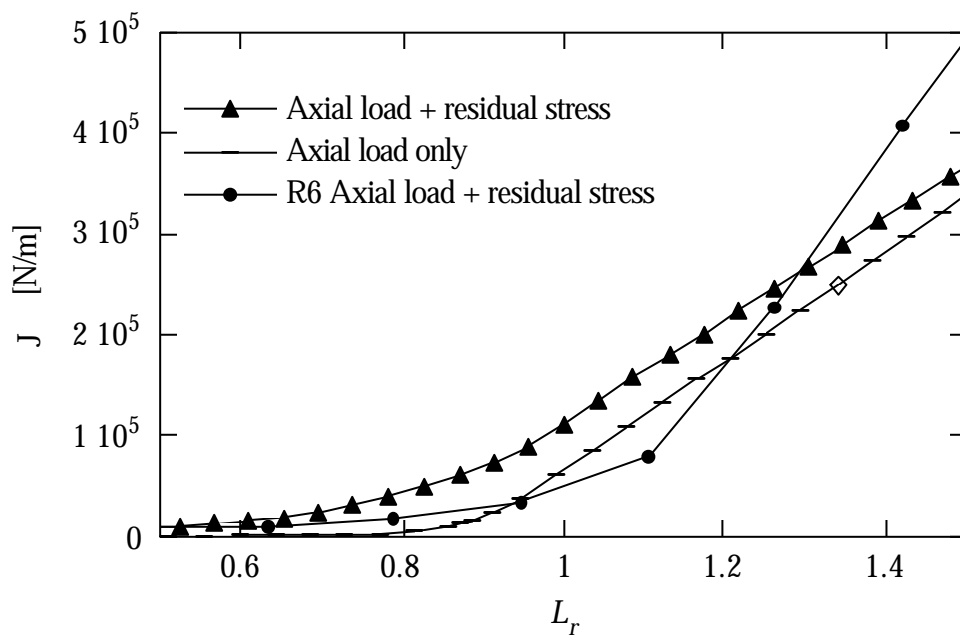


**Figure 3** The displacement  $d$  of the end of the pipe is plotted against the applied load  $P$  at the end of the pipe. The point determined by the intersection of the two tangent lines represents the limit point for excessive yielding i.e. when  $P = P_g$ . The  $P - d$  curve if the hardening vanishes is also plotted. The corresponding limit load then becomes 192 MPa. The limit load solution,  $P_g = 162$  MPa, was obtained from the handbook [4].

The following three graphs show the comparisons of  $J$  (figure 4),  $CTOD$  (figure 5), the relative contribution from residual stresses to  $J$  and  $CTOD$  (figure 6), during axial loading.

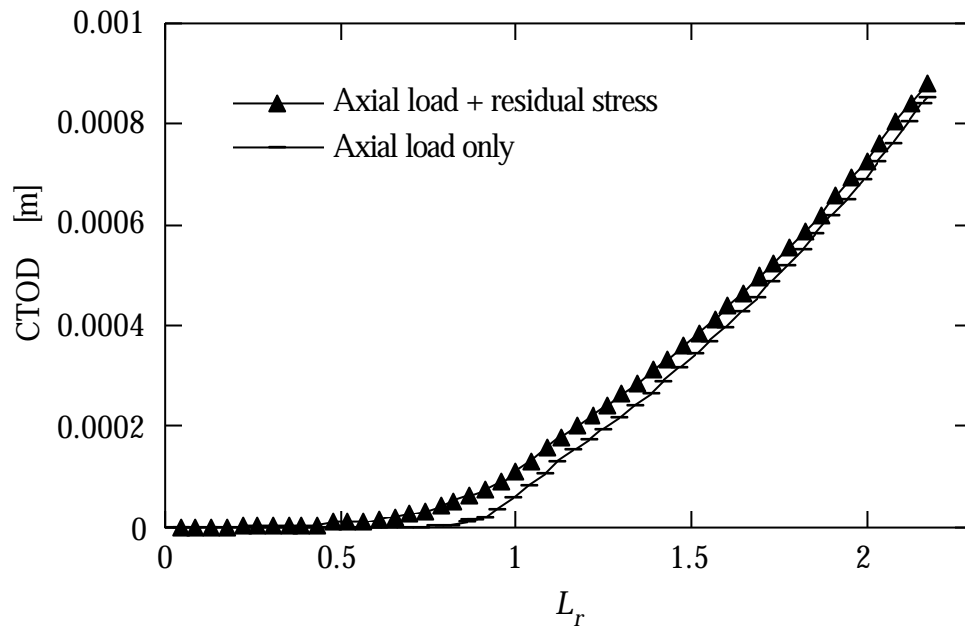


a)

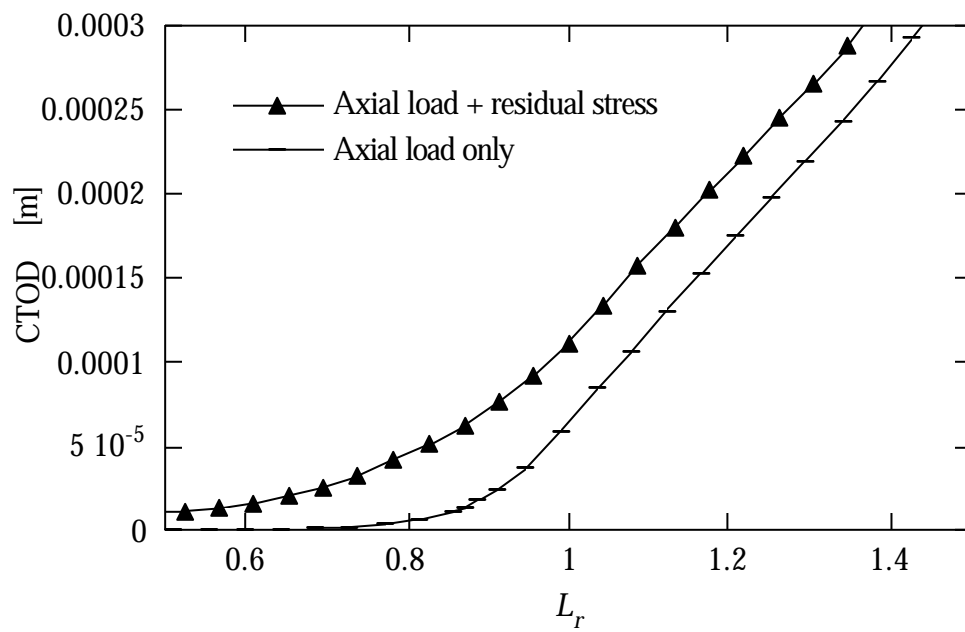


b)

**Figure 4** a) The  $J$ -integral as a function of  $L_r$ . The  $J$ -values are evaluated at the tenth contour i.e. a ring with a radius of nine elements from the cracktip.  
 b)  $J - L_r$  resolved for load values closer to  $L_r = 1.0$ .

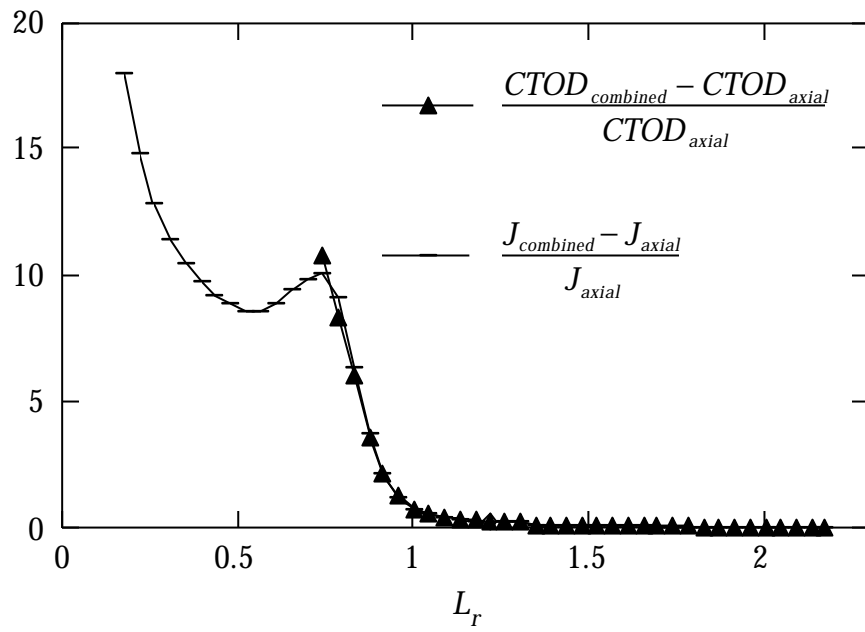


a)

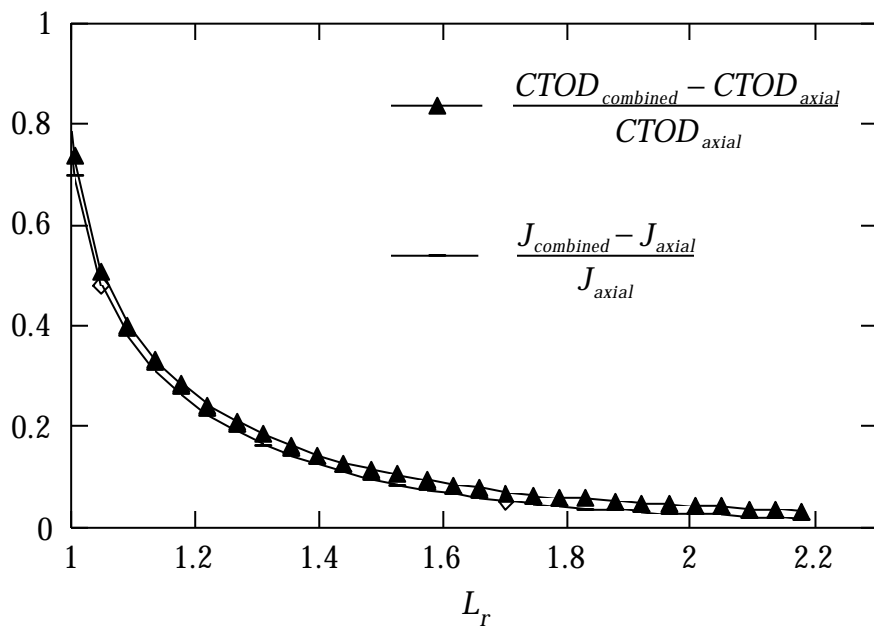


b)

**Figure 5** a) The *CTOD* as a function of  $L_r$ .  
 b) *CTOD* -  $L_r$  resolved for load values closer to  $L_r = 1.0$ .



a)



b)

**Figure 6** a) The relative difference of  $J$  and  $CTOD$  with and without residual stresses.  
b) Close up for better resolution for high  $L_r$ .

The principal behaviour of the  $J$ -integral is as expected for primary loads. The curve in figure 4 is essentially composed of an elastic part and a plastic part with a steep slope, c.f. Bergman [15] for a review on differences between primary and secondary loads. The results of Kumar et al [16] are quite similar, though they used a thermal load as secondary load, see Appendix A for details and a discussion of their results.

An evaluation of the case of combination of an axial load and residual stresses according to the R6-procedure is also included in figure 4. The R6-procedure gives a slightly non-conservative estimation between  $L_r = 0.95$  and  $L_r = 1.2$ . However it should be remembered that  $L_r$  is not defined by a limit load equal to 162 MPa as would normally be the case in a standard handbook solution, such as [4], instead a definition of the limit load equal to 228 MPa based on fully plastic behaviour, as shown in figure 3, is used. In Appendix D the corresponding results of figure 4, where  $L_r$  is based on a limit load equal to 162 MPa, are shown.

It is interesting to quantify the relative contribution from the residual stresses during axial loading for both the  $J$ -integral and the  $CTOD$ . In figure 6 the relative differences between  $J$  with both residual and axial stresses present,  $J_{combined}$ , and  $J$  with only axial stresses present,  $J_{axial}$ , are shown. The same type of quantity formed with  $J$  replaced by  $CTOD$ , is plotted in figure 6. The  $CTOD$  could not be evaluated for  $L_r$  less than about 0.7 for the case with only axial loading despite the fine mesh. The irregular behaviour for the case with both residual stresses and axial stresses present for  $L_r$  less than about 0.8 can be explained by path dependency of  $J$  at low axial load levels, which is a result of the stress history due to crack growth. The close coincidence of the  $J$ -curves and the  $CTOD$  curves in figure 6 suggests that the relation in equation (4) holds. This suggests also that  $J$  can be a possible fracture parameter if the integration contours are not far from the crack-tip. However only an experimental investigation can give a definite answer to the question of whether  $J$  or  $CTOD$  can be useful fracture parameters during this type of loading situation with residual stress- and strain-fields present. In Appendix B a short review is given on the specific problems encountered when residual stresses are present.

The results support the experiments in ref. [5-9]. The contribution to the fracture parameters from the residual stresses is negligible for large  $L_r$  as shown in figure 6b. The contribution from the residual stresses decreases rapidly between  $L_r = 0.8$  and  $L_r = 1.3$ . For  $L_r = 1.3$  the contribution of the residual stresses is 20% of the axial load contribution. For  $L_r = 1.6$  the contribution of the residual stresses is about 6%. An important observation is that this makes it essential to have a reliable value for  $L_r$  when plastic failure occurs i.e. when  $L_r = L_r^{max}$ . In the present investigation the value of  $L_r$  at plastic collapse can not be defined. This is due to the linear hardening material model adopted (with its bilinear representation). Reasonably close to  $L_r = 1.0$  the results should be valid also for other type of hardening behaviour. However, the results should be viewed with caution if a quantitative

conclusion is desired. This is because the results are qualitative in the sense that a particular geometry and material model are chosen in this work.

The parameter  $d$  is shown in figure 7 for the load cases with and without residual stresses. The non-dimensional parameter  $d$  is defined through the relation, c.f. Shih et al [14],

$$CTOD = d \frac{J}{S_s}. \quad (4)$$

In [14], however, a Ramberg-Osgood material was considered, which makes their results quantitatively incomparable with ours.

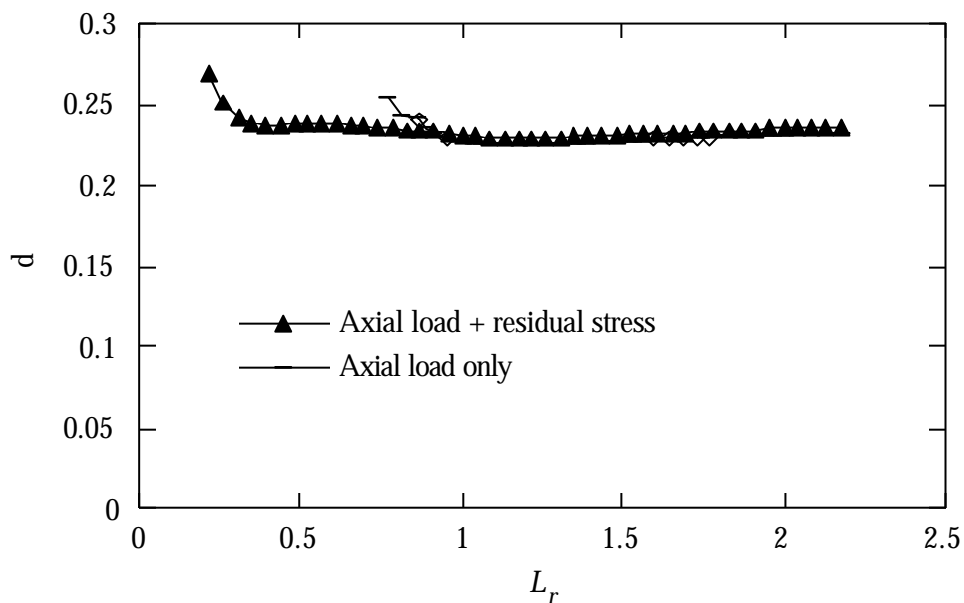


**Figure 7** The values of the non-dimensional parameter  $d$  as a function of  $L_r$ . The parameter  $d$  is defined according to equation (4).

The values of  $d$  in figure 7 for both the case with the residual stresses present and the case with only axial stresses, are scattered very little from the value 0.23. This means that at least in this investigation the J-integral is well defined through equation (4) with  $d = 0.23$ . However remember that for  $J$  evaluated with remote contours the J-integral seems definitely path dependent. Appendix B provides a discussion of this problem. The reason for the cut-off at  $L_r = 0.8$  for the case of axial loading only is that  $CTOD$  could not be evaluated even with the fine mesh used. The corresponding cut-off for the case of both axial loading and residual stresses is  $L_r = 0.25$ . In this case  $CTOD$  may be undefined because of the crack growth prior to the application of axial loading, see Appendix B.

### 3.2 Relaxation of residual stresses due to unloading

To investigate the effect of relaxation, several unloadings were performed for the uncracked geometry from different axial load levels, see figure 8. The stress distribution along the symmetry line may serve as an input in an engineering estimation e.g. a fracture assessment according to the R6-procedure. It is not relevant to unload the cracked pipe since the  $J$ -integral and the  $CTOD$  become meaningless in this type of unloading situations.

The resulting levels of the residual stress distributions, after unloading, decreases with increasing  $L_r$ , and does not change for load levels larger than  $L_r = 0.8$ . For a circumferential surface crack, on the inside of the pipe, not deeper than 40% of the wall-thickness, there will clearly be only very small residual stresses after unloading from a high level of axial load. The stress peak of 80 MPa for the case  $L_r = 0.8$  is located about 70% of the wall thickness from the inside of the pipe, through the wall.

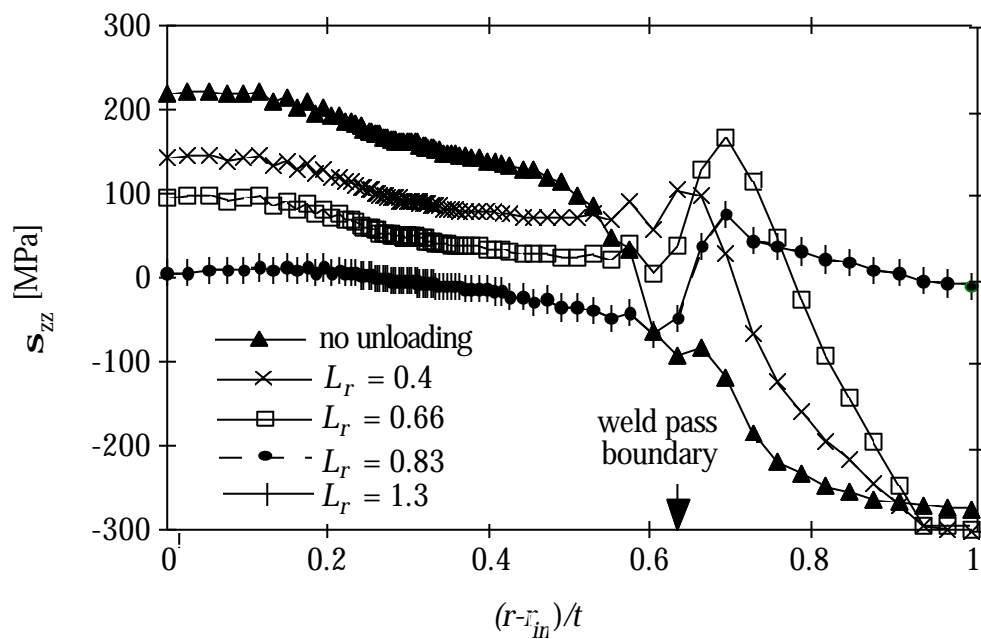


**Figure 8** The axial stresses at the symmetry line after unloading. The  $L_r$ -values represent the different load levels from which the unloadings were performed.

### 3.3 Different tangent modulus.

The chosen bi-linear kinematical hardening material model limits the analyses in two ways. It can only approximately account for the more realistic non-linear hardening behaviour of materials. Secondly, a point

of plastic collapse can not be defined, in our notation, this means that no  $L_r^{max}$  exists. This section addresses those limitations.

In order to get some understanding of how these limitations affect conclusions, a series of runs was performed on the same pipe geometry. The material models were the same except for a different tangent modulus,  $E_T$ . The residual stresses,  $CTOD$  and  $J$ , the relative differences,  $(J_{combined} - J_{axial})/J_{axial}$  and  $(CTOD_{combined} - CTOD_{axial})/CTOD_{axial}$  were calculated and the results are shown in figure 9 - 12.

In figure 9 it can be seen that for  $E/E_T = 0.0001$ , which is nearly perfectly plastic material behaviour, the residual stresses attain the highest tensile stress level. The stress distribution changes shape somewhat but the stress level does not change very much with different amount of hardening. Note however that close to the inside of the pipe the stresses are fairly independent of the tangent modulus.

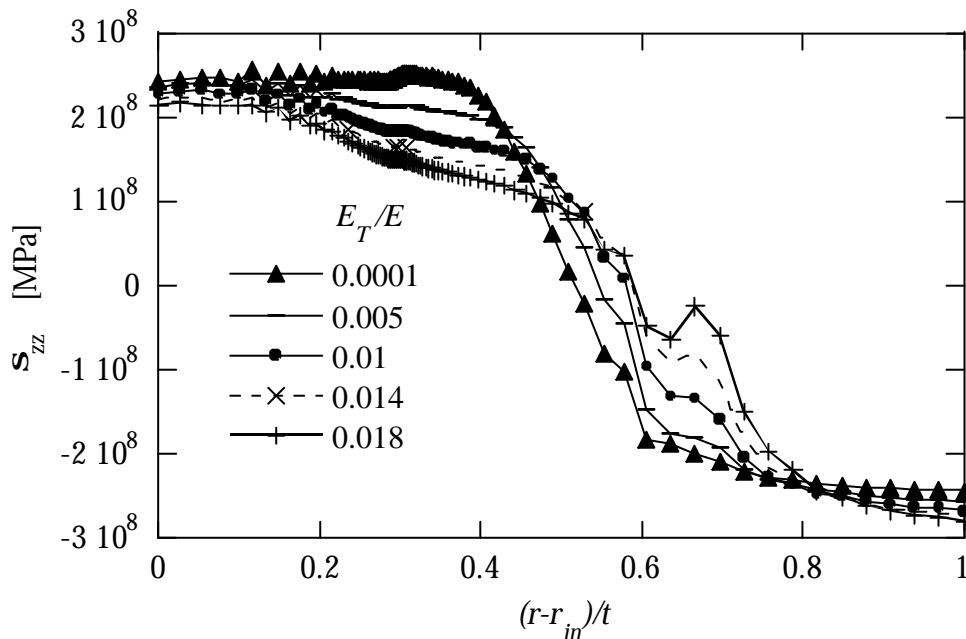


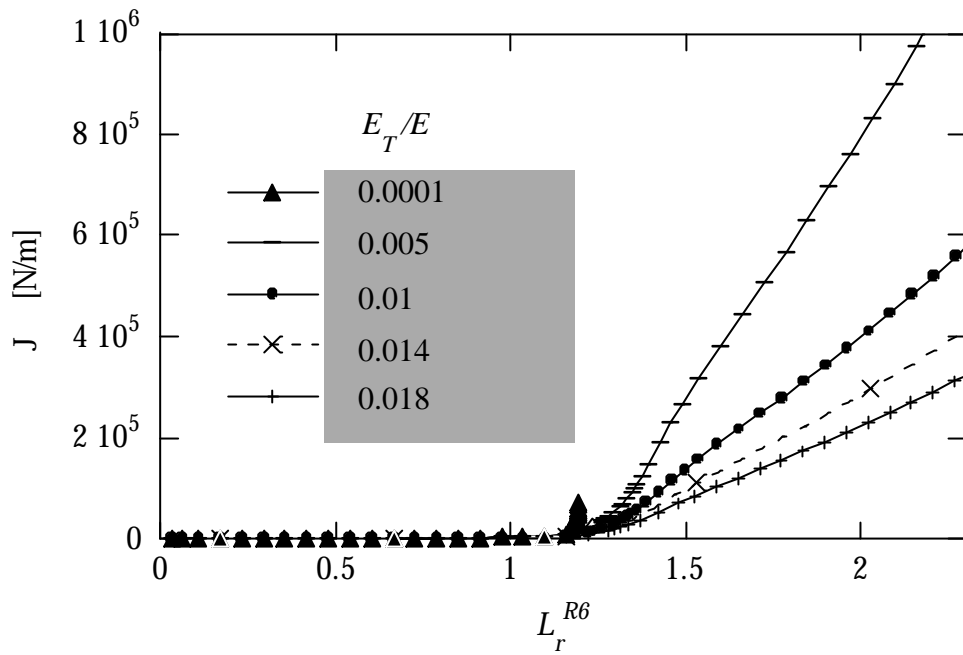
**Figure 9** Axial residual stresses in the weld centerline for  $E_T/E = 0.0001$ , 0.005, 0.01, 0.014, 0.018.

The limit load  $P_g$  definition, with graphical determination, used in section 3.1 is not appropriate here. In order to compare  $J$  and  $CTOD$  using the same scale,  $L_r$  is defined as  $L_r^{R6} = P/P_g^{R6}$  where  $P_g^{R6}$  is the limit load used in R6 and in the handbook [4].

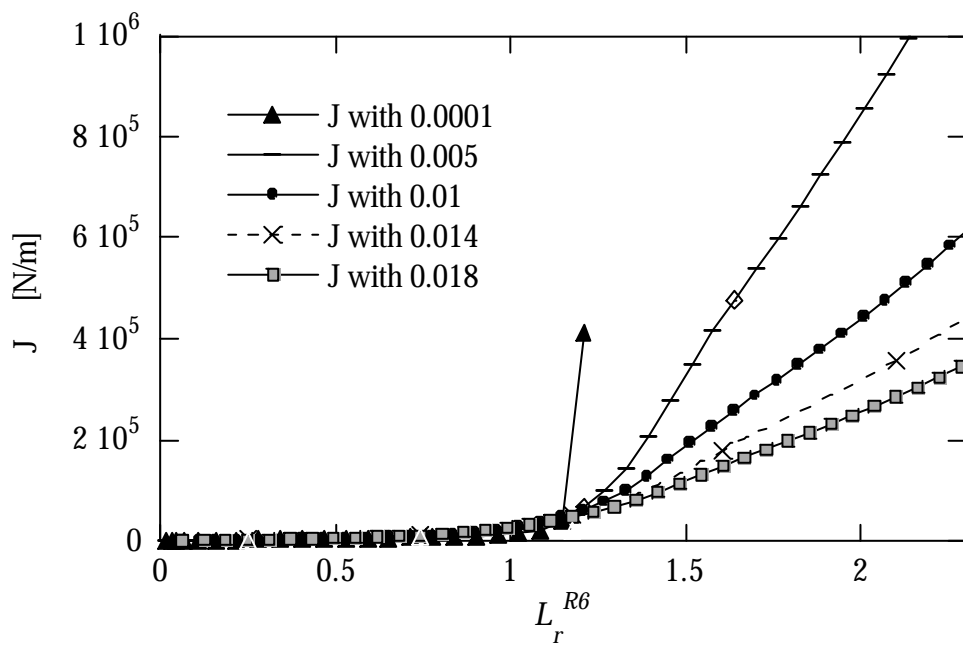
For the same  $L_r$  -value more plasticity is introduced with decreasing hardening. This is consistent with the behaviour of the  $J - L_r$  and the  $CTOD - L_r$  curves, figure 10 - 11, which rise steeper with decreasing hardening

The relative differences of  $J$  and  $CTOD$ , figure 12, vanishes at a higher rate the lower the hardening is. For  $E/E_r = 0.0001$  there is no curve because  $L_r$  does not get higher than  $L_r = 1.25$  because of widespread plasticity.

The lowering of hardening has thus the effect of reducing the contribution from the residual stress to  $J$  or  $CTOD$ . In a real material the same should occur as  $L_r$  approaches  $L_r^{\max}$ . This implies that not only does the contribution from residual stresses decrease with increasing  $L_r$  but that also an additionally decreasing effect due to decreasing hardening, should be taken into account for high  $L_r$  - values.

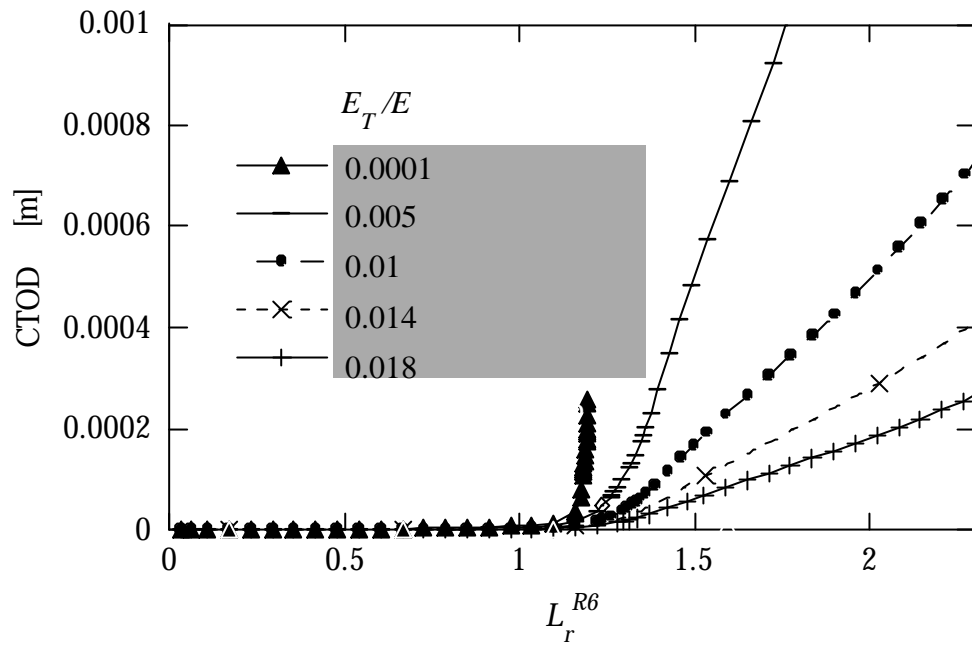


a)

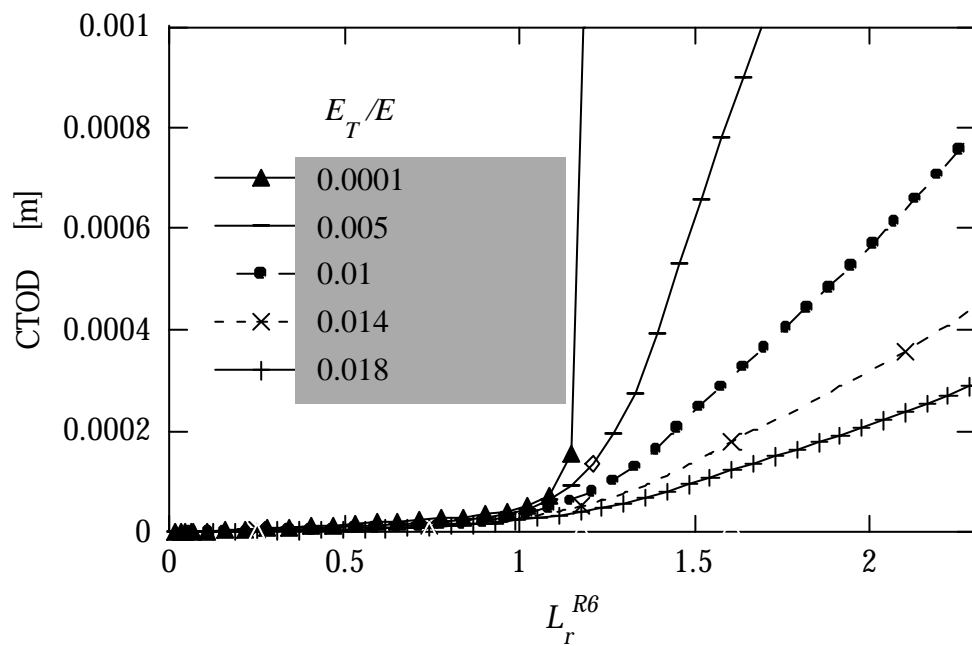


b)

**Figure 10** a)  $J_{axial}$ , (axial load only), as a function of  $L_r$  for different  $E_T/E$ .  
 b)  $J_{combined}$ , (axial load and residual stresses), a function of  $L_r$  for different  $E_T/E$ .

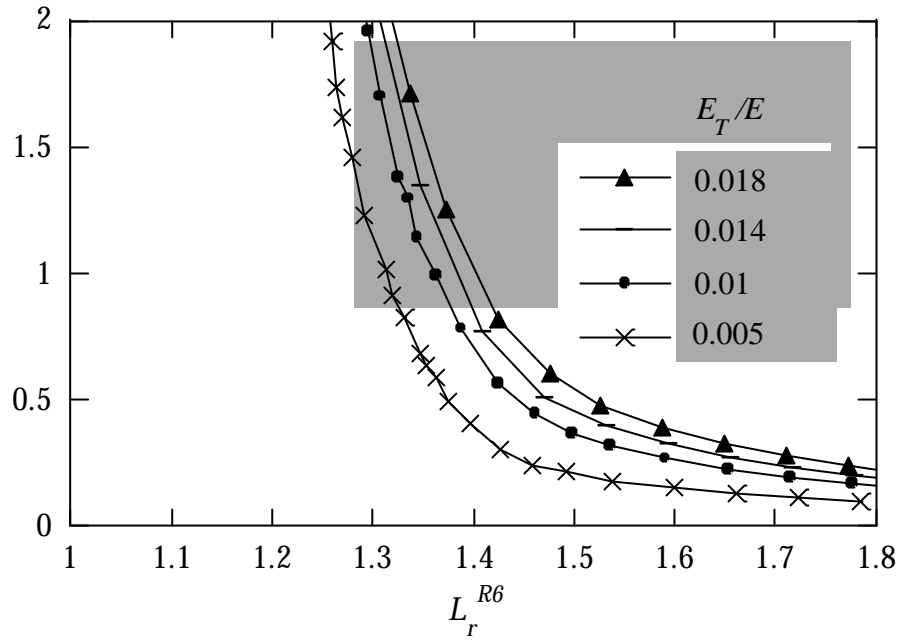


a)

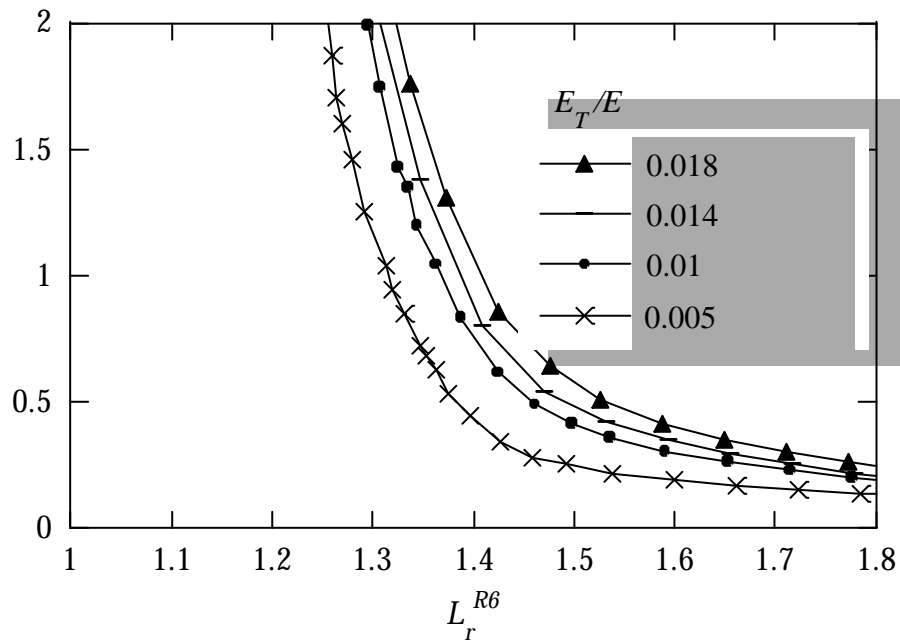


b)

**Figure 11** a)  $CTOD_{axial}$ , (axial load only), as a function of  $L_r$  for different  $E_T/E$ .  
 b)  $CTOD_{combined}$ , (axial load and residual stresses), a function of  $L_r$  for different  $E_T/E$ .



a)

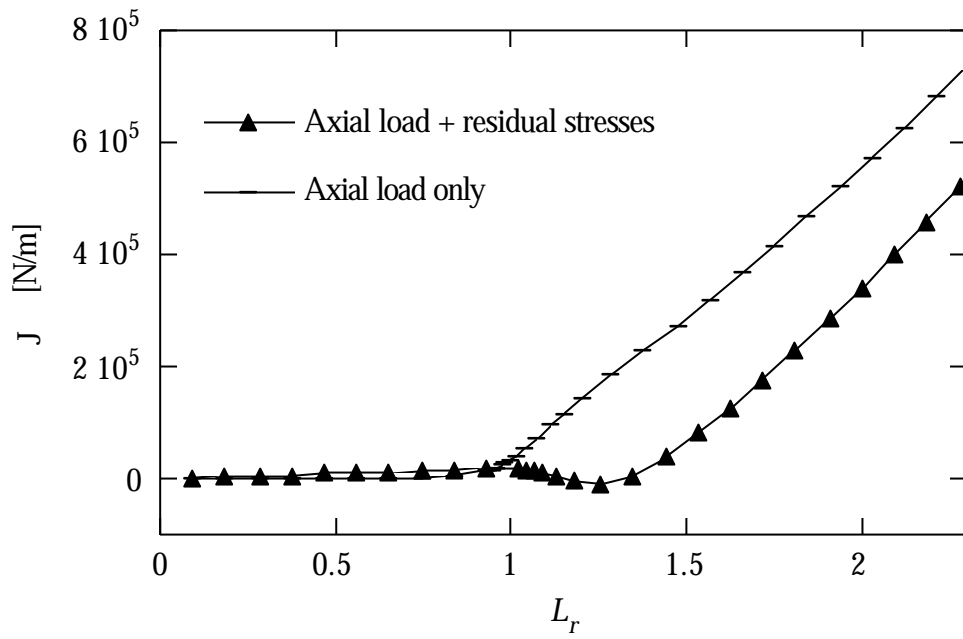


b)

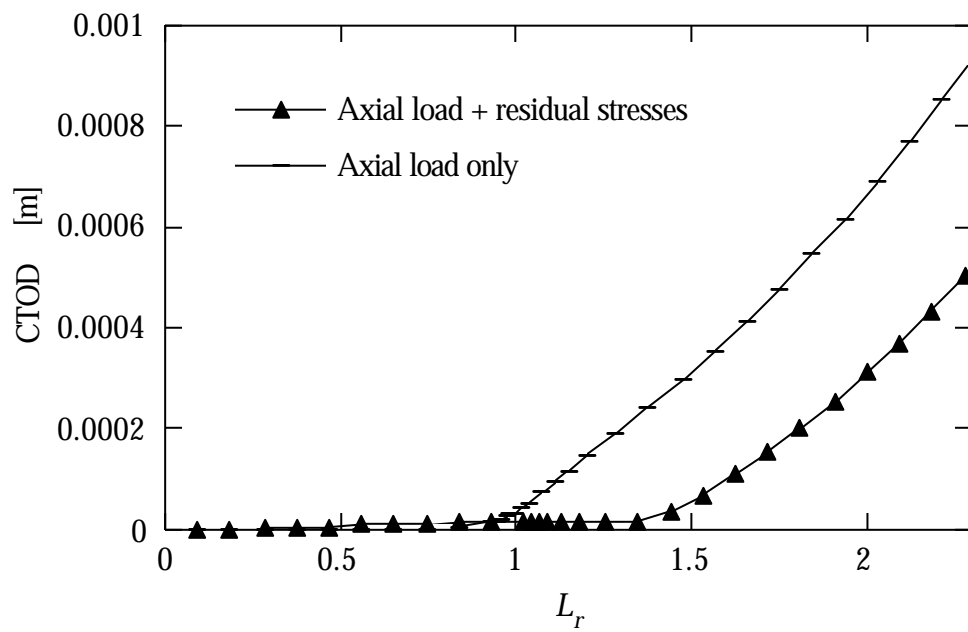
**Figure 12** a) The quantity  $(J_{combined} - J_{axial}) / J_{axial}$  as a function of  $L_r$  for different  $E_T/E$   
 b)  $(CTOD_{combined} - CTOD_{axial}) / CTOD_{axial}$  as a function of  $L_r$  for different  $E_T/E$

### 3.4 The effect of using linear isotropic hardening in the calculation of $J$ and $CTOD$

Although a very exact model of the hardening behaviour during welding certainly would be very complex, including both expansion and translation of the yield surface in stress space, it is believed that kinematic hardening models the plastic behaviour better than isotropic hardening. To study the effect of the chosen hardening model, the  $J$ -integral and  $CTOD$  were also calculated assuming linear isotropic hardening with and without weld residual stresses during axial loading of the pipe. It is seen in figure 17 that the choice of hardening behaviour is important. When using isotropic hardening, the stresses are unloaded close to the crack-tip during part of the loading history. This is reflected in the negative  $J$ -values at  $L_r = 1.25$ . In fact for  $L_r = 1$  it would be more favourable to include the residual stresses than not to include the residual stresses. The trend for  $CTOD$  is the same. The results are similar to those of Hou et al. [2], who also used an linear isotropic hardening model. In Appendix A, the contribution of thermal stresses to  $J$  was studied. An isotropic hardening model was used, but the corresponding  $J - L_r$  curves do rather follow each other in the same manner as the kinematic hardening model in the case of residual stresses. The behaviour seen in figure 13 can not be observed in Appendix A. The explanation of this must be found in the way the residual stresses and thermal stresses are generated. The major difference between residual stresses and the thermal stresses used in Appendix A is that the residual stresses are due to the residual strains left when all thermal loading is gone, whereas the thermal load in Appendix A is active throughout the loading history (applied internal pressure). Also, no crack growth took place in Appendix A, which means less load cycling. The residual stresses are present only in the welding and nearby, while the thermal stresses are distributed in the whole pipe.



a)



b)

**Figure 13** a) The  $J$ -integral as a function of  $L_r$ , with isotropic hardening  
 b) The  $CTOD$  as a function of  $L_r$ , with isotropic hardening

#### 4. A WELDED PIPE SUBJECTED TO A THERMAL LOAD

A thermal load was applied to the pipe with a circumferential surface crack both with and without the residual stresses present. The thermal load was imposed by specifying a radial temperature distribution in the pipe according to

$$T(r) = 22.5 - n \cdot \exp(r - r_i) \cdot \frac{(r - (r_i + t))}{t}, \quad (5)$$

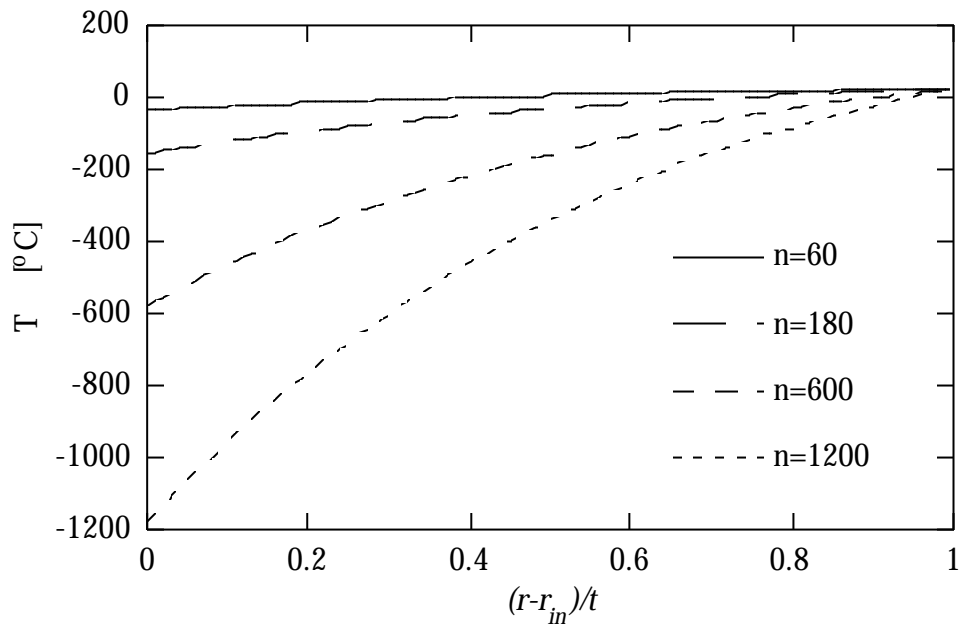
which is presented together with the resulting axial stresses for the linear elastic case in figure 14. As the thermal load was increased in very small steps by increasing the value of the scaling parameter  $n$  in equation (5), the J-integral and the *CTOD* were calculated. A limit load parameter can not be defined for the type of secondary thermal load used here since the pipe can not yield completely. The thermal load at which the innermost fibre begins to yield may serve as a point of reference. This occurs when

$$\frac{EaDT}{(1-n)s_Y} = 1.27, \quad (6)$$

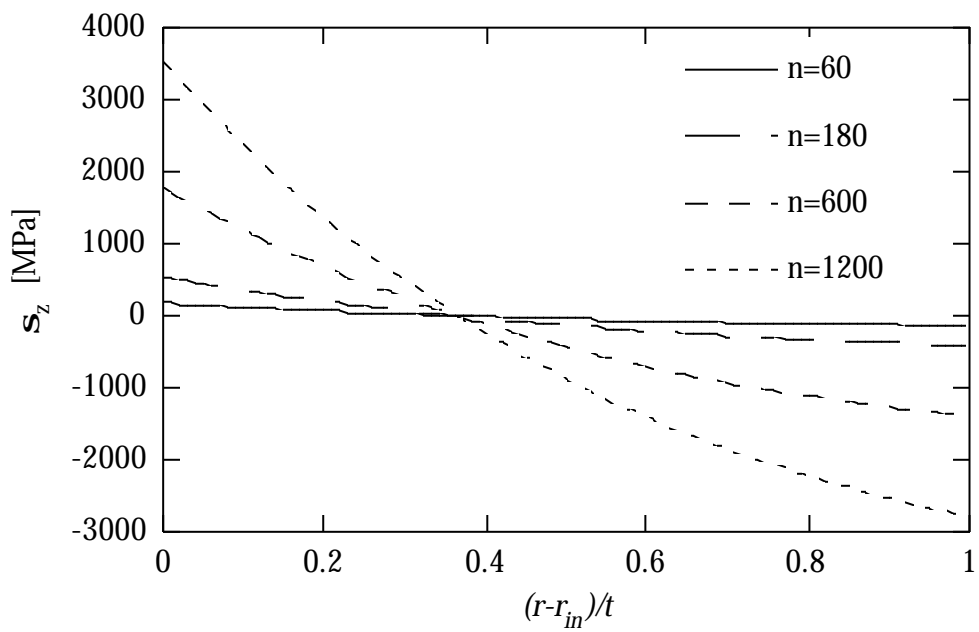
where  $DT = 20^\circ\text{C} - T$ , i.e. the difference in temperature between room temperature and the temperature  $T$  at  $r = r_i$  in equation (5).

The figures 10, 11 and 12 show the comparisons of  $J$ , *CTOD* and  $d$  respectively, for the different temperature distributions, shown in figure 14 a), with and without the residual stress present. The behaviours of  $J$  and *CTOD* are similar. They are related through the non-dimensional parameter  $d$  according equation (4). In figure 17 it is shown that the value of  $d$  is 0.23, which is the same as determined for the case of axial loading.

The loading curves for  $J$  and *CTOD* are very different from the corresponding curves for the pipe subjected to an axial load. This is because the thermal load is secondary and cannot cause plastic collapse. There is always a portion of the pipe cross section that does not yield. An important consequence of this is that the contribution of the residual stresses is approximately constant in absolute terms during the increase of the thermal load. The smallest contribution of residual stresses is found for low load levels. It must be remembered, however, that for low load levels the values of  $J$  are less reliable because of the effect of crack growth prior to loading.

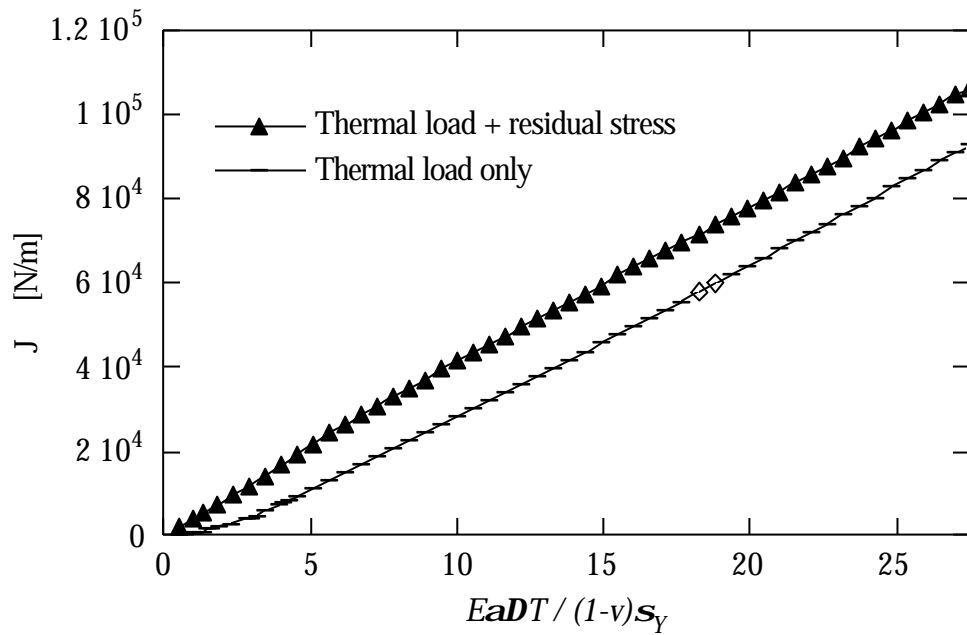


a)

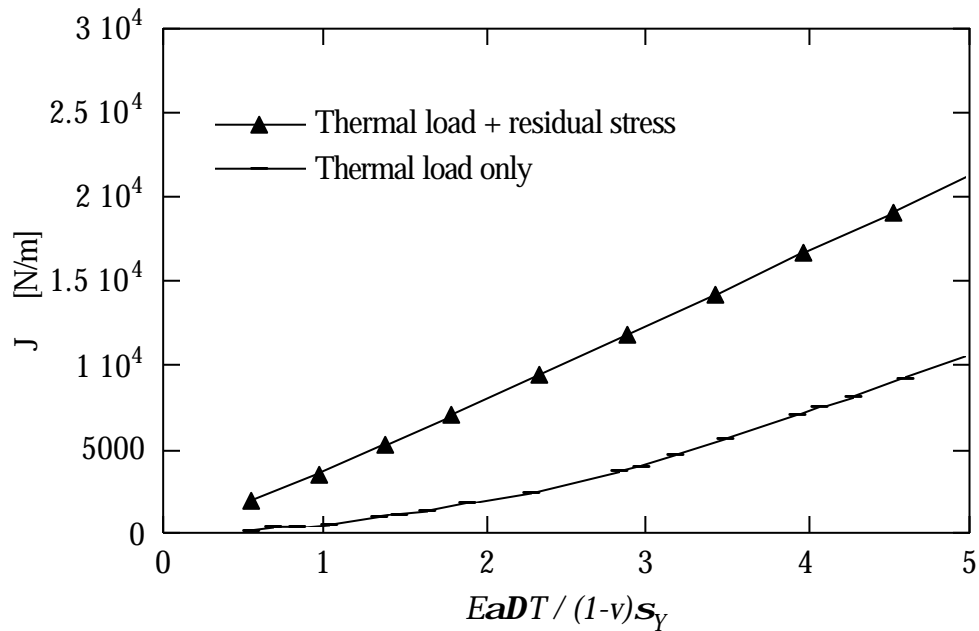


b)

**Figure 14** a) The temperature distribution according to equation (5) through the thickness of the pipe.  
 b) The corresponding axial stress distribution for the linear elastic case through the thickness of the pipe.

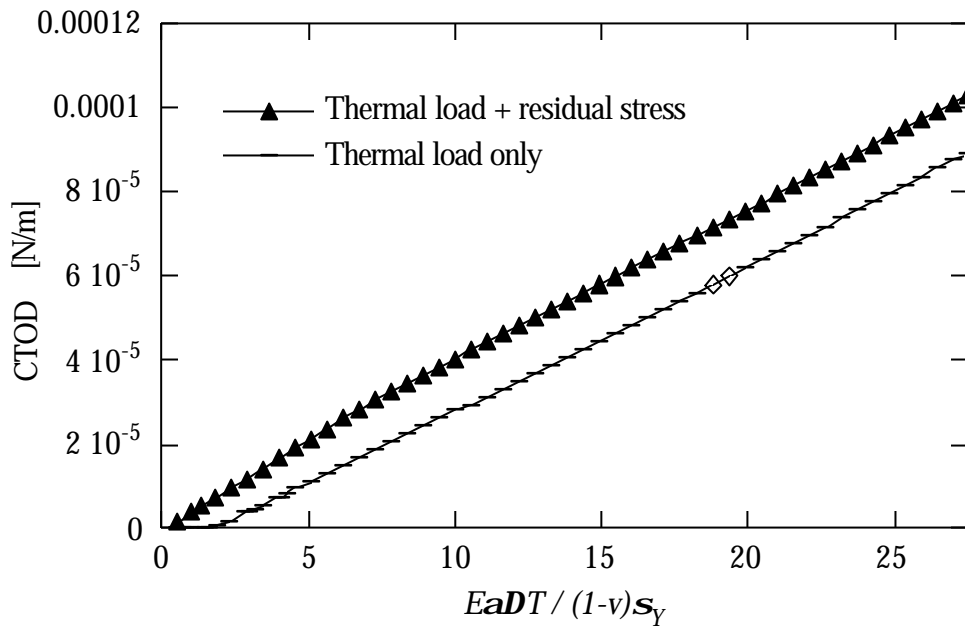


a)

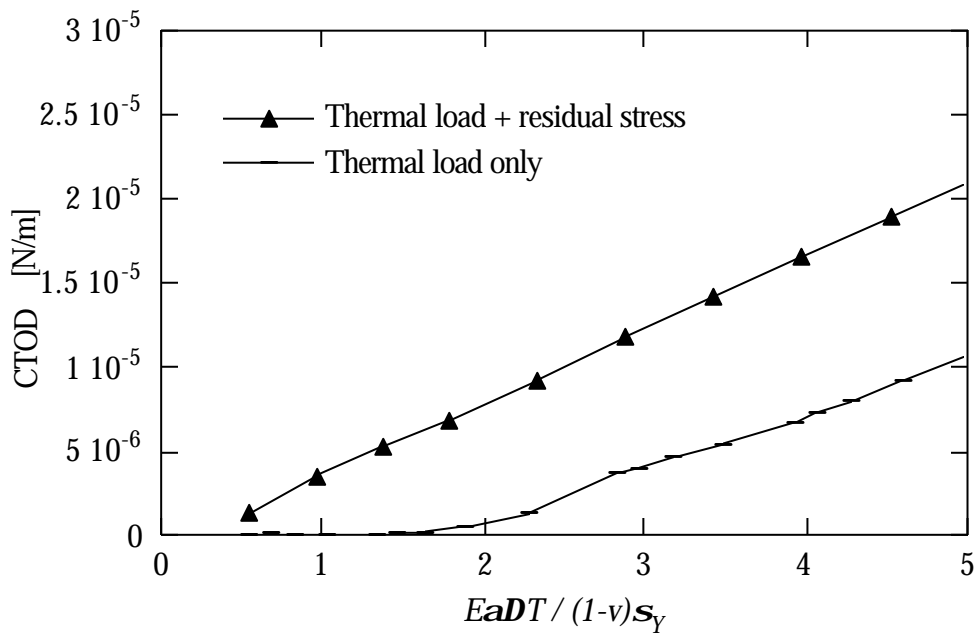


b)

**Figure 15** a)-b) The  $J$ -integral as a function of the non-dimensional load parameter  $E\alpha DT / (1-\nu)s_Y$ .



a)



b)

**Figure 16** a)-b) The *CTOD* as a function of the non-dimensional load parameter  $E a \Delta T / (1 - \nu) s_Y$ .

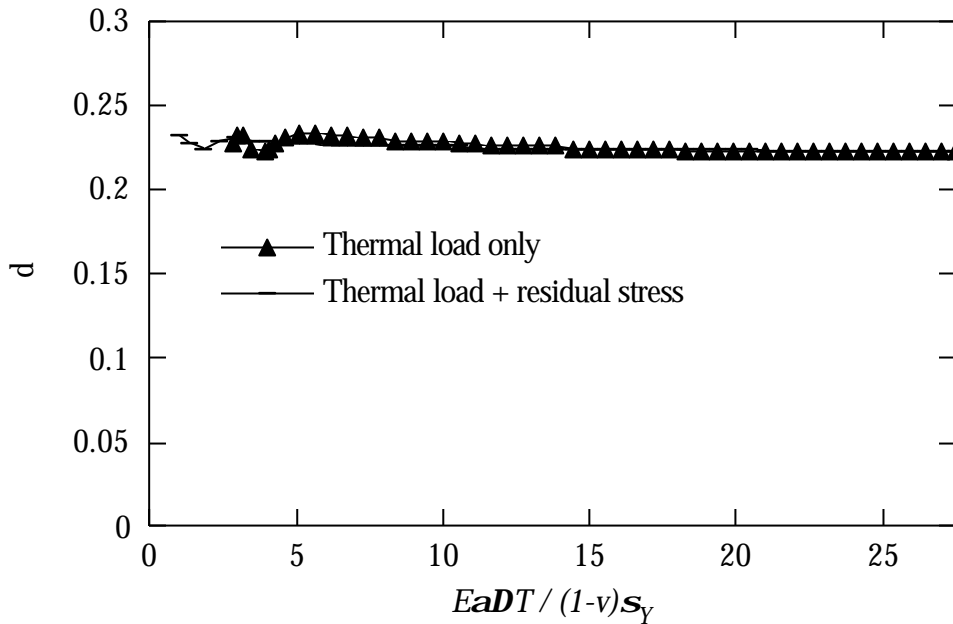


**Figure 17** The values of the non-dimensional parameter  $d$  as a function of  $L_r$ . The parameter  $d$  is defined according to equation (4).

## 5. DISCUSSION

The main result of the present study is shown in figure 6. The relative contribution as defined in fig. 6 from the residual stresses to  $CTOD$  or  $J$  decreases rapidly between  $L_r = 0.8$  and  $L_r = 1.3$ . For  $L_r = 1.25$  the relative contribution from the residual stresses is 20% compared to the axial load. For very high  $L_r$ -values the contribution becomes negligible. Thus, for the particular pipe studied the contribution of the residual stresses is negligible only for very high values of  $L_r$ . However, because of the linear hardening material model adopted (with its bilinear representation), plastic collapse can not be defined. This means that we do not know for a particular value of  $L_r$ , exactly how far the load is from a fully plastic situation corresponding to true plastic collapse.

In the work by Kumar et al [16] the contribution of a thermal load to the  $J$ -integral during a mechanical loading has been studied. They concluded that thermal loads can be neglected for high mechanical loads. In Appendix A a verification and extension of their result is presented. A corresponding analysis made with a much more severe thermal loading than in [16] showed that the contribution to  $J$  from the thermal stresses can be significant also for  $L_r$  larger than 1. In this case, the value of  $L_r$  must be raised to more than 1.4 for the relative contribution from the thermal stresses to be small.

Green et al [6] proposed that residual stresses need not to be included in fracture assessments of austenitic steels if  $L_r$  is larger than the ratio of the 1% proof stress to the 0.2% proof stress. In the present study this would correspond to an  $L_r$  -value of about 1.1. The present investigation indicates that this limit should be larger, approximately  $L_r = 1.3$ . If it can be shown that instability in a ductile material occurs beyond this limit, the weld residual stresses may be ignored, at least for estimation of the crack size or load at instability.

In our opinion great care must be taken in the treatment of the contribution of welding residual stresses or thermal stresses in fracture assessments. The present results with proper simulation of the weld-induced stresses do support the idea of giving weld residual stresses a lower weight in a fracture evaluation if high primary loads are present. However, the limit of  $L_r$  at which the relative contribution from weld residual stresses (or thermal loads) to  $CTOD$  or  $J$  is small enough, is likely to depend on the particular material model, crack geometry and the shape and level of the residual (or thermal) stress distribution. At present, there is insufficient evidence to make a general quantitative recommendation. A natural continuation of this work is therefore to extend the investigation to other crack geometries and material models.

## 6. CONCLUSIONS

- If  $CTOD$  can successfully be used in fracture analyses of welded components, the conventional  $J$ -integral seems also to be a useful parameter in numerical analyses, for analysing welded components. This is true at least if  $J$  is evaluated for contours very near the crack tip in a refined mesh.
- For the studied case, the relative contribution from the weld residual stresses to  $CTOD$  or  $J$ , decreases rapidly for high values of  $L_r$ . For  $L_r = 1.25$  the relative contribution from the residual stresses is 20% compared to the axial load. For very high  $L_r$  -values the contribution becomes negligible. This is believed to be valid qualitatively also for other material models, crack geometries and residual stress distributions.
- The exact limit of  $L_r$  at which the relative contribution from welding residual stresses (or thermal stresses) to  $CTOD$  or  $J$  is sufficiently small to be neglected is likely to depend on the particular material model, crack geometry and the shape and level of the residual (or thermal) stress distribution. This conclusion is supported by the results in Appendix A where two different crack geometries are studied. To some extent this limit of  $L_r$ , where the contribution from residual stresses becomes negligible, is also depending on the definition of the limit load. Therefore, at present there is insufficient evidence to make a general quantitative recommendation.

- The contribution from residual stresses does decrease for high  $L_r$  as shown in this study. A linear kinematic hardening model was used. However, in a real material the hardening is non-linear and  $E/E_T$  decreases with  $L_r$ . It was found, by varying the slope of the hardening curve, that an additionally decreasing effect on the contribution from residual stresses to  $CTOD$  or  $J$  due to the decreasing hardening, should be taken into account for high  $L_r$  -values.
- The choice of hardening model is important. It is believed that kinematic hardening is a better choice than isotropic hardening in low cycle simulations i.e. in a few-pass welding process, as in the present study.
- For the case of weld residual stresses in combination with high thermal stresses, it is found that the plasticity induced by the thermal stresses is not sufficient to suppress the influence of weld residual stresses on  $CTOD$  or  $J$ , even for very high thermal loads.
- The residual stresses can be relaxed by unloading from a primary tensile load. Unloading from a load level corresponding to  $L_r = 0.83$  will result in almost a complete relaxation of the weld residual stresses for the studied case.

## REFERENCES

- [1] BRICKSTAD, B. and JOSEFSON, B. L. (1996), *A parametric study of residual stresses in multipass butt-welded stainless steel pipes*, SAQ/FoU-Report 96/01 SAQ Kontroll AB, Stockholm, Sweden
- [2] HOU, Y. C., KIM, M., PAN, J. and BRUST, F.W. (1996), *Effects of residual stresses on fracture of welded pipes*, Residual Stresses in Design, Fabrication, Assessment and Repair, ASME, PVP-Vol. 327, 67-75
- [3] KANNINEN, M. F., BRUST, F. W., AHMAD, J. and ABOU-SAYED, I. S. (1982), *The numerical simulation of crack growth in weld-induced residual stress fields*, Residual Stress and Stress Relaxation, Plenum Publishing Corporation, 227-248
- [4] ANDERSON, P., BERGMAN, M., BRICKSTAD, B., DAHLBERG, L., NILSSON, F. and SATTARI-FAR, I. (1991), *A procedure for safety assessment of components with cracks - Handbook.*, SAQ/FoU-Report 96/08, SAQ Kontroll AB, Stockholm, Sweden
- [5] GREEN, D. and KNOWLES, J. (1994), The treatment of residual stress in fracture assessment of pressure vessels, *Journal of Pressure Vessel Technology*, Vol. 116, 345-352
- [6] GREEN, D., SHARPLES, J. K. and STEWART, G.(1993), *Experimental evidence in support of proposals for the treatment of residual stress in fracture assessment of pressure vessels*, Pressure Vessel Integrity, ASME, PVP-Vol. 250, 1-9
- [7] SHARPLES, J. K., SANDERSON, D. J., BOWDLER, B. R., WIGHTMAN, A. P. and AINSWORTH, R. A. (1995), *Experimental programme to assess the effect of residual stresses on fracture behaviour*, Fatigue and Fracture Mechanics in Pressure Vessels and Piping, ASME, PVP-Vol. 304, 539-551
- [8] SHARPLES, J. K., HARRISON, M., MAY, K. A., CHIVERS, T. C. and SMITH, E. (1993), *The effect of residual stresses on fracture behaviour*, Pressure Vessel Integrity, ASME, PVP-Vol. 250, 105-113
- [9] SHARPLES, J. K. and GARDNER, L. (1996), Ductile tearing tests of 316 stainless steel wide plates containing weldments, *International Journal of Pressure Vessels & Piping*, Vol. 65, 353-363

- [10] ASME XI (1986), Task Group for Piping Flaw Evaluation, *ASME Journal of Pressure Vessel Technology*, Vol. 108, 352-366
- [11] MILNE, I., R. A. AINSWORTH, A. R. DOWLING and A. T. STEWART (1987), *Assessment of the integrity of structures containing defects*. CEGB Report R/H/R6 - Revision 3, Central Electricity Generating Board, Berkeley, England, updated and maintained by Nuclear Electric Ltd, Gloucester, England, 1997
- [12] ABAQUS (1995), *Users manual*, version 5.5, Hibbit, Karlsson and Sorenson, USA.
- [13] ARGYRIS, J. H., SZIMMAT, J., and WILLIAM, K. (1983), *Finite element analysis of the arc welding process*, Numerical methods in thermal problems- Proceedings of the third international conference, Seattle WA, USA, Pineridge press, Swansea UK, 249-258.
- [14] SHIH, C. F. (1981), Relationship between the  $J$ -Integral and the crack opening displacement for stationary and extending cracks , *Journal of Mechanics and Physics of Solids*, Vol. 29, 305-326
- [15] BERGMAN, M. (1991), *A fracture mechanical analysis of secondary stresses-part 1*, SAQ/FoU-Rapport 94/03 (in Swedish), SAQ Kontroll AB, Stockholm, Sweden
- [16] KUMAR, V., SCHUMACHER, B.I. and GERMAN, M.D. (1991), An engineering approach for examining crack growth and stability in flawed structures, *Computers and structures*, Vol. 40, 487-501
- [17] RICE, J. R. (1968), A path independent integral and the approximate analysis of strain concentration by notches and cracks, *Journal of Applied Mechanics*, Vol. 35, 379-386
- [18] DRUGAN, W. J., RICE, J. R. and SHAM, T-L. (1982), Asymptotic analysis of growing plane strain tensile cracks in elastic-ideally plastic solids, *Journal of Mechanics and Physics of Solids*, Vol. 30, 447-473, Erratum in Vol. 31.
- [19] ANDERSON, T. L. (1991), *Fracture mechanics, fundamentals and applications*. CRC Press, Boca Raton, USA.

## APPENDIX A. EPRI/GE 'S TREATMENT OF THERMAL STRESSES

Non-linear finite element analyses have been performed on the contribution from thermal stresses to the J-integral under increasing mechanical loading. The geometries and some of the load cases are those of Kumar, Schumacher and German [16]. The shorthand notation KSG will be used for their work throughout this Appendix. The von Mises yield criterion and associated flow rule is used together with isotropic hardening and a bilinear representation of the stress strain curve. The geometrical and material data are as follows:

- Geometries: 1) A single edge notched tension SEN(T) panel with  $a/t = 0.25$  and  $t = 5.8$  mm.
- 2) A cylinder with the dimensions  $a/t = 0.5$ ,  $t = 50.8$  mm,  $R_i/t = 10$  with a complete circumferential surface crack on the inside subjected to internal pressure.

Materials:  $\sigma_Y = 414$  MPa,  $E = 207$  GPa,  $E/E_t = 70$ .

The thermal loading was introduced prior to the mechanical loading to high levels. The objective is to study the contribution from thermal stresses to the J-integral as the mechanical loading increases. The thermal distribution used in KSG varies with the distance through the thickness,  $x$ , according to

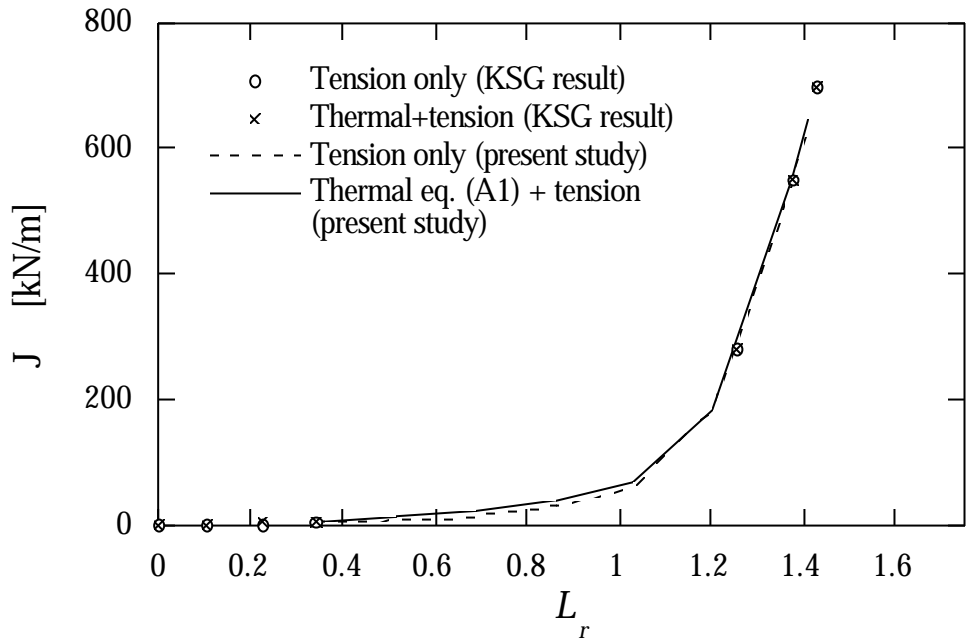
$$T(x) = \mathbf{a} [93.33 + 195 (x/t) - 49 (x/t)^2] \quad (\text{A1})$$

where  $\mathbf{a} = 1$  for the SEN(T) panel and  $\mathbf{a} = 0.25$  for the cylinder. In figure A1, i.e. the KSG case, it is observed that the thermal load is very low. Therefore more severe thermal load cases for both the plate, equation (A2), and the cylinder, equation (A1), with  $\mathbf{a} = 2$  were studied.

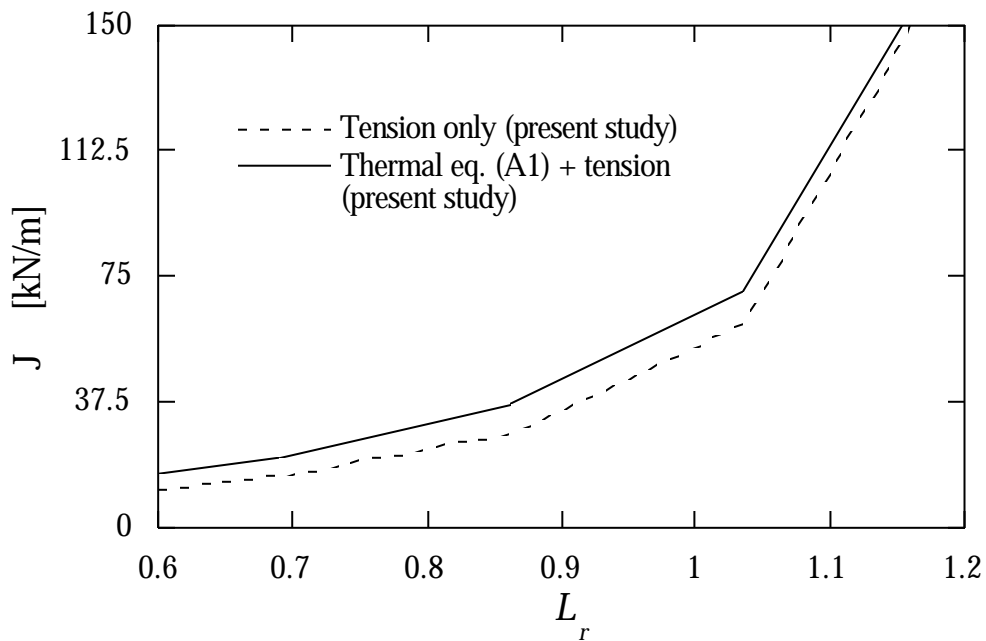
$$T(x) = 1000 [4(x/t) - 6(x/t)^2 + 3(x/t)^3] \quad (\text{A2})$$

The results in KSG did not coincide with our results when the mechanical loading was large. However, with the hardening ten times higher than reported in KSG where  $E/E_t = 7$ , i.e.  $E/E_t = 70$ , the results agree very well with our calculations. It therefore, appears that there is a misprint in KSG and the hardening should be  $E/E_t = 70$ . The same misprint was found also for the cylinder. As a consequence of these findings the hardening is set to  $E/E_t = 70$  in all of the calculations performed.

The mechanical load levels are expressed in terms of the limit load parameter  $L_r$ . The definition of  $L_r$  for the cylinder and SEN(T) specimen can be found in Andersson et al [4].



a)



b)

**Figure A1** a)-b) The  $J$ -integral as a function of  $L_r$  for the SEN(T) specimen with  $a/W = 0.25$  and  $\sigma_Y = 414$  MPa. The thermal load is that of KSG, equation (A1), with  $\alpha = 1$ .

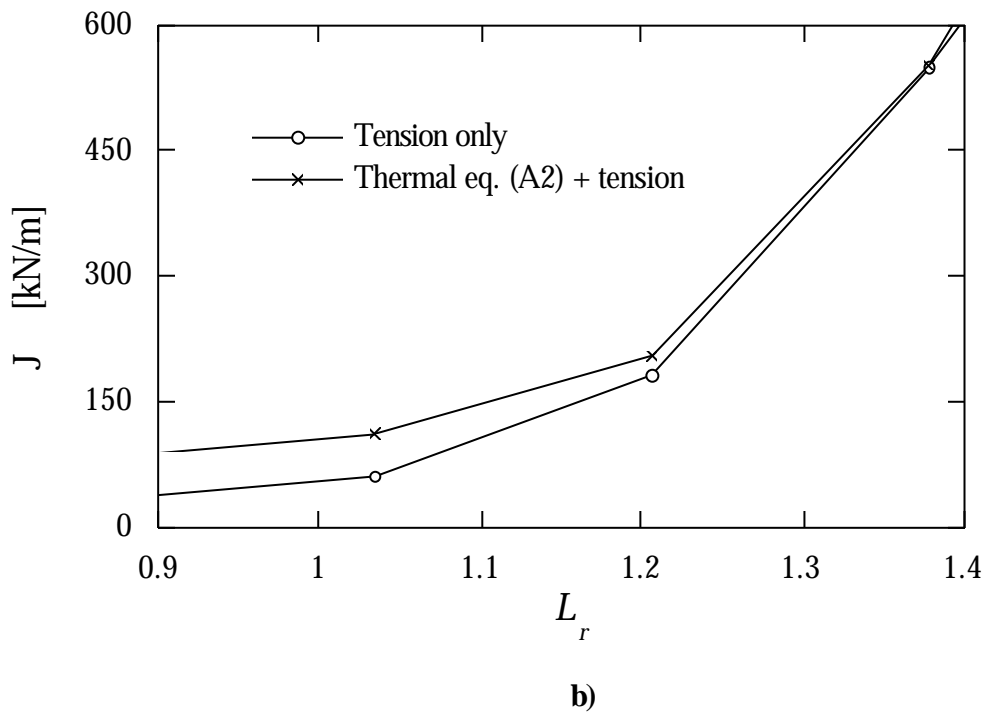
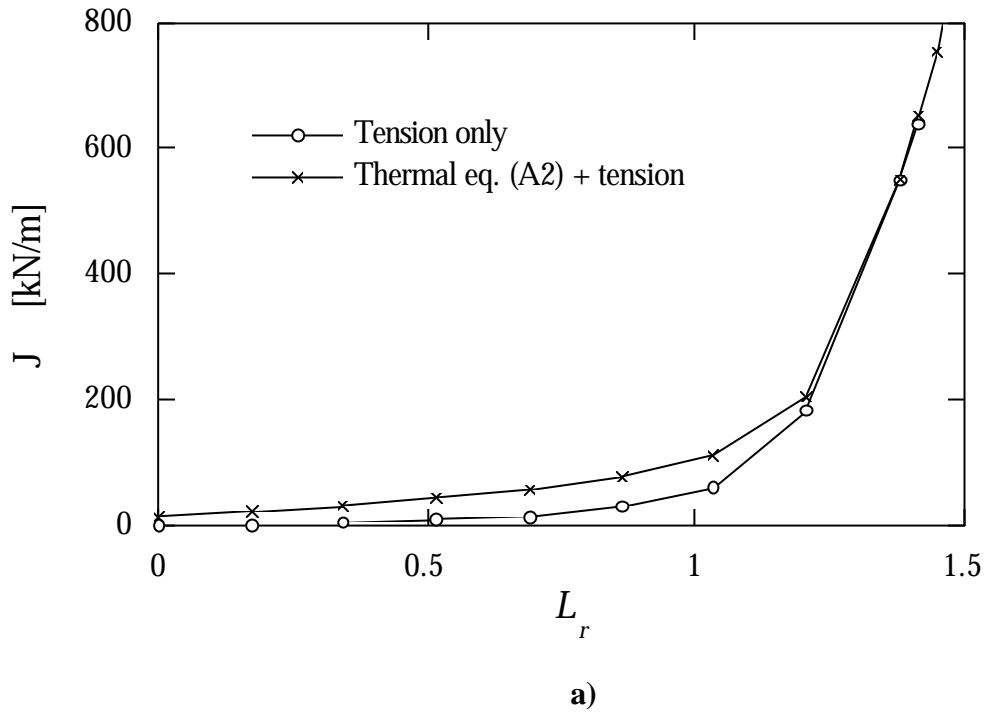
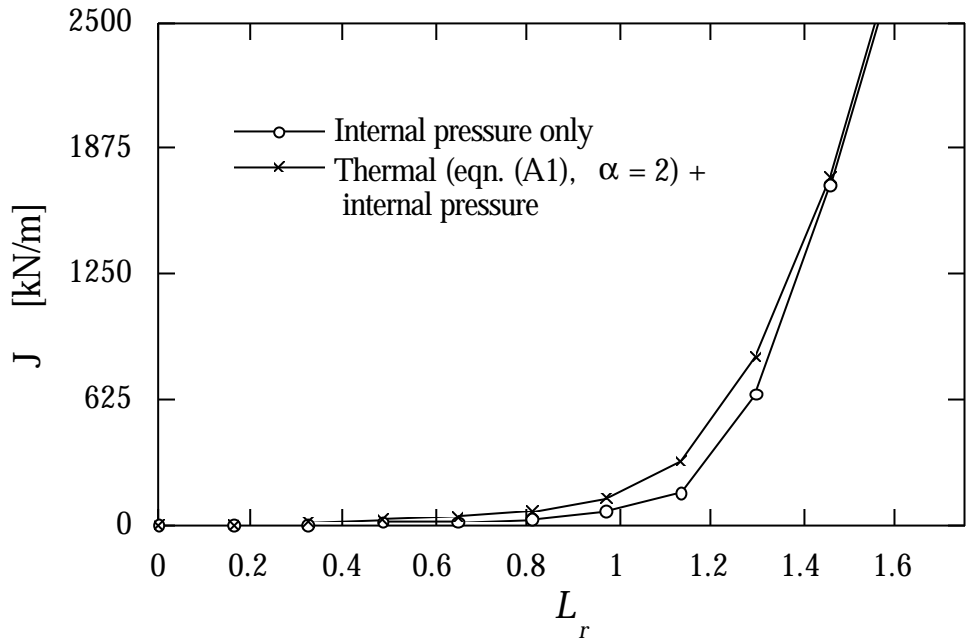
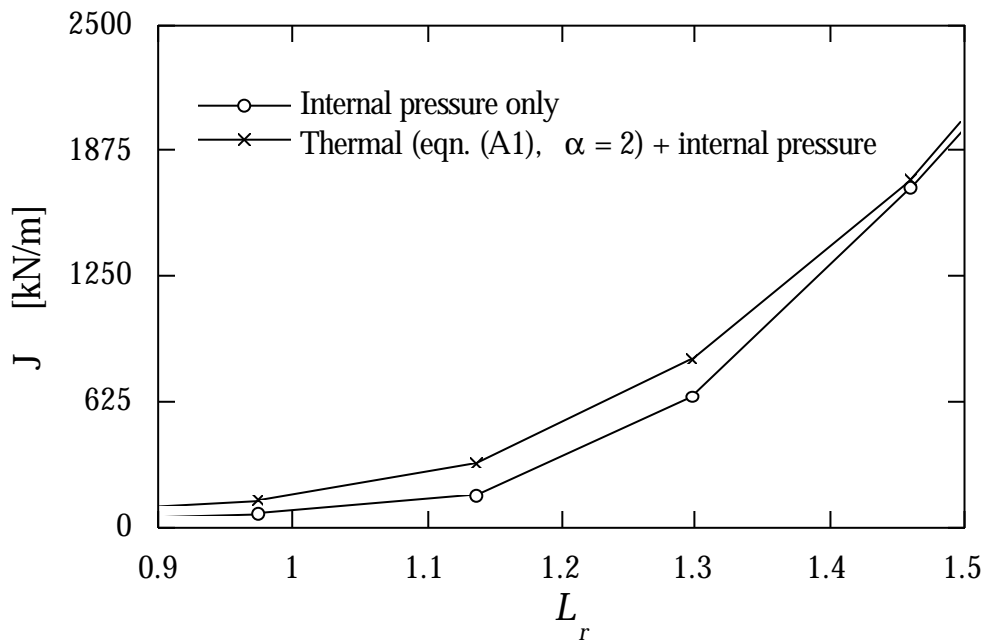


Figure A2. a)-b) The  $J$ -integral as a function of  $L_r$  for the SEN(T) specimen with  $a/W = 0.25$  and  $S_Y = 414$  MPa. The thermal load is the result of the temperature distribution in equation (A2) which is more severe than in figure A1.



a)



b)

**Figure A3** a)-b) The  $J$ -integral as a function of  $L_r$  for the cylinder with  $a/t = 0.5$ ,  $t = 50.8$ ,  $R/t = 10$  and  $\sigma_y = 414$  MPa. The thermal load is the result of the temperature distribution in equation (A1) with  $\alpha = 2$ , which is more severe than in figure A1.

It can be observed in figure A1 that for  $L_r$  larger than 1.1 the thermal contribution is almost zero. In figure A2 a more severe thermal load was used and subsequently the contribution from the thermal stress is more pronounced. The value of  $L_r$  must be above 1.2 to be negligible. The  $J$ -  $L_r$  curves for the cylinder are presented in figure A3. The value of  $L_r$  at which the contribution from the thermal stresses to the  $J$ -integral can be neglected is above 1.4. Thus the different geometries and thermal loads used have a significant influence on the  $L_r$  -value at which the contribution from the thermal load to  $J$  can be neglected. This is an important observation because this limits the ability to recommend a specific value above which the contribution from secondary stresses (in this case a thermal load) to the  $J$ -integral can be neglected.

## APPENDIX B. THE $J$ -INTEGRAL AND THE $CTOD$ AS FRACTURE PARAMETERS

The  $J$ -integral introduced by Rice [17] in 1968 was derived using a non-linear elastic material model to account for plasticity (deformation theory plasticity). As long as the loading is monotonically increasing and no unloadings occur, i.e. the loading is proportional, Rice'  $J$ -integral is applicable also for incremental plasticity models. The  $J$ -integrals as a function of integration contours for a stationary crack are shown for the axial load in figure B1 and for the thermal load defined by equation (5) in figure B2. The first integration contour is the crack-tip itself, the second contour is the closest ring of elements around the crack-tip and the third contour is the ring of element closest to the second contour and so on. In the figures B1-B2 it is shown that the  $J$ -integral values are fairly path independent for the stationary crack.

The welding process causes a highly non-proportional load situation. Thus the  $J$ -integral is not applicable for a crack experiencing loading during a welding process. Instead we have considered a crack which has grown subcritically (IGSCC or fatigue) influenced by the residual stresses after the completion of the welding process.

The growth of a crack is a non-proportional load situation and the  $J$ -integral becomes path dependent. Furthermore the crack opening profile of a quasistatically growing crack is very different from a stationary crack, c.f. Drugan, Rice and Sham [18], which makes it practically impossible to measure  $CTOD$ . After the crack has stopped an axial tensile load is applied. During the loading a plastic redistribution of stresses may occur in the regions with weld-induced strains, this redistribution is likely to result in a non-proportional load situation, giving a meaningless  $J$ -integral.

However, the path dependency, whether it originates from the crack growth or the redistribution of stresses, may become a minor disturbance when sufficient monotonic load (thermal or mechanical) is applied to the stationary crack. This seems to be the case when a kinematic hardening model is used. For the isotropic hardening model, however, the redistribution of stresses has a substantial effect also at late stages in the loading history. The crack-tip even experiences unloading at a certain stage, see figure 17.

It can be observed in the figures B3 and figure B4, that even for quite high load levels, the  $J$ -integral becomes strongly path dependent from about contour number 20. On the other hand  $J$  seems fairly path independent for contours within contour number 20. It is only for very large load levels that  $J$  becomes practically path independent for all contours.  $CTOD$  was evaluated as described in Appendix C and  $J$  was evaluated for the tenth contour throughout this paper. A relation, equation (4), between  $J$  and  $CTOD$  was established, The correlation between  $J$  and  $CTOD$  remained approximately constant as the axial load was increased, as can be seen in figure 7.

An explanation of the path dependence of  $J$  for contours a certain distance away from the crack-tip may be connected to the way the  $J$ -integral is calculated in ABAQUS [12], where initial strains and strain-induced residual stresses are not considered. However, ABAQUS takes into account thermally induced stresses when calculating the  $J$ -integral. The problem in our case is that the crack is not present during the welding process, in other words ABAQUS cannot take into account thermally induced strains that was produced before the crack was introduced. This can be one part of the explanation why the  $J$ -integral is path independent within contour 20, which is less than 1 mm from the crack-tip. Within that distance, the singular stress field dominates the residual stresses. Thus the contribution of the residual stresses to the  $J$ -integral becomes small and the  $J$ -integral calculated in ABAQUS becomes path independent.

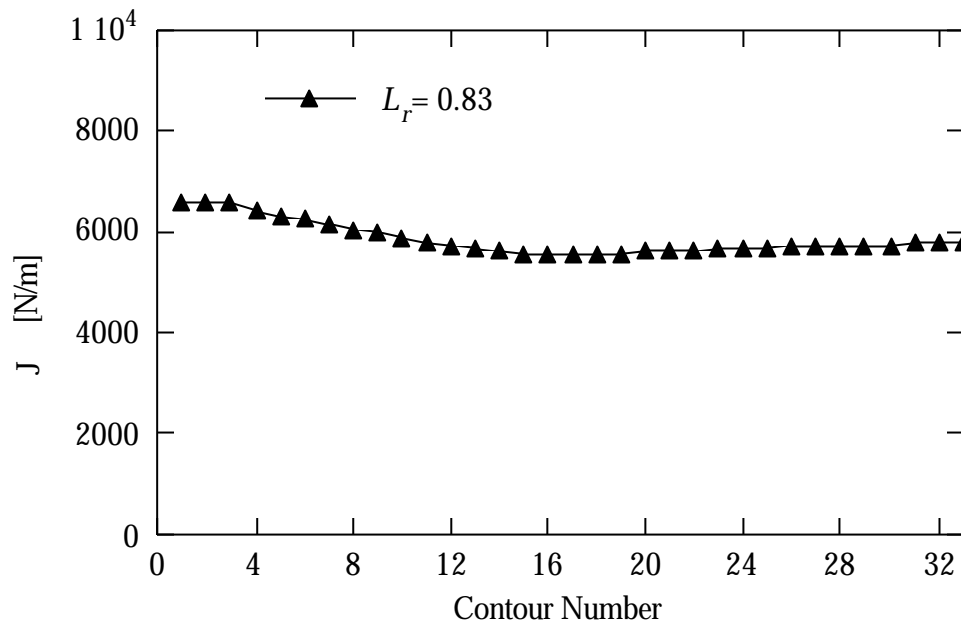


**Figure B1** The  $J$ -integral values for 33 different contours of integration for the pipe in axial tension only.

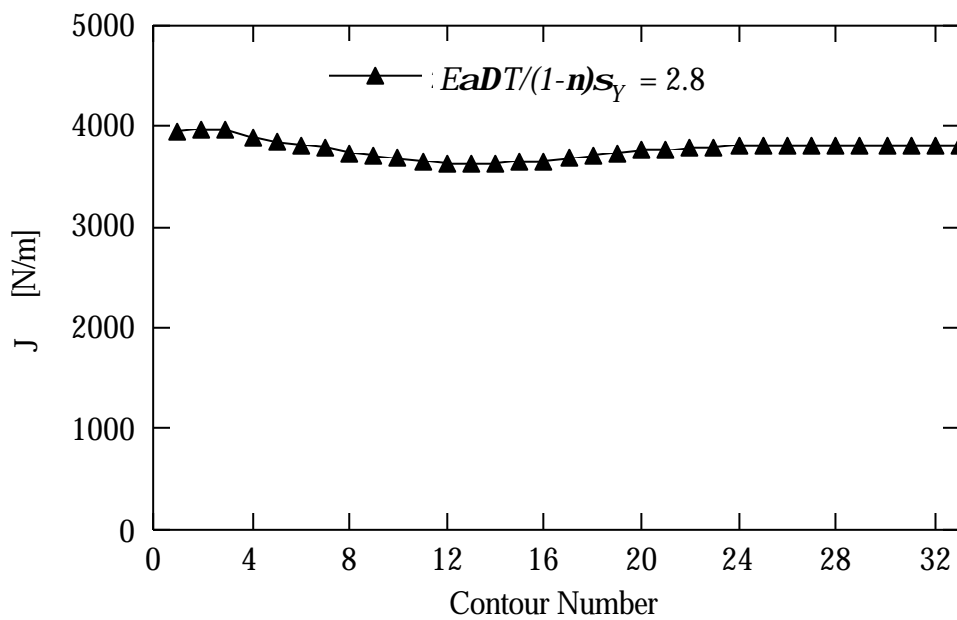


**Figure B2** The  $J$ -integral values for 33 different contours of integration for the pipe subjected to thermal loading only according to equation (5).

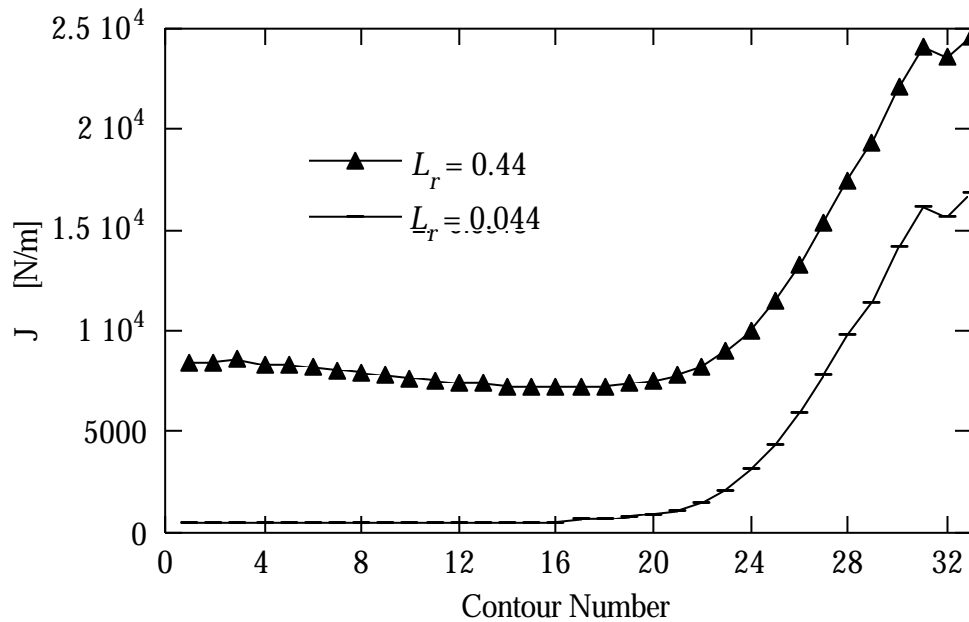
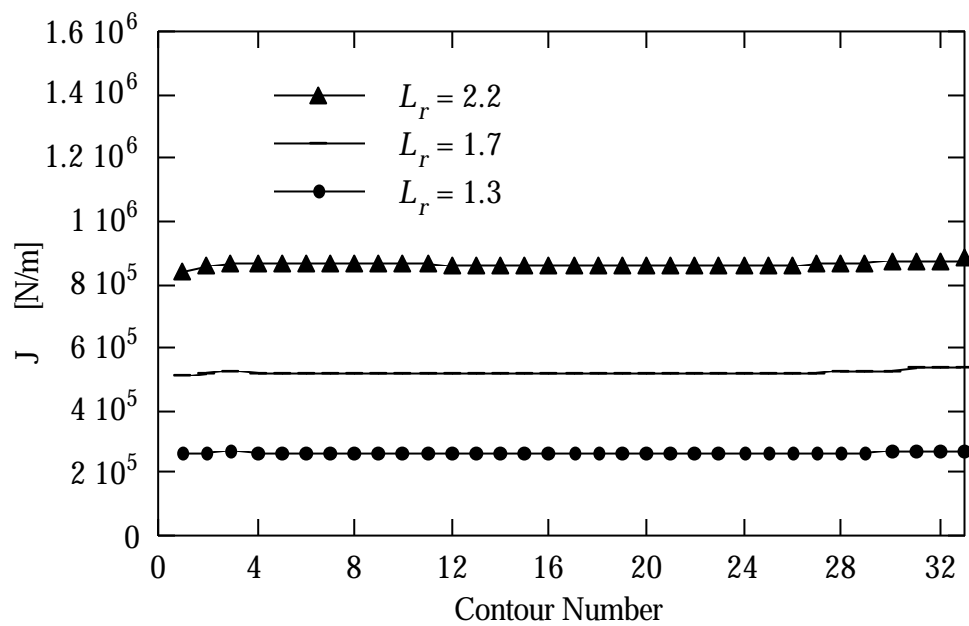


**Figure B3** The  $J$ -integral values for 33 different contours of integration for the welded pipe in axial tension.

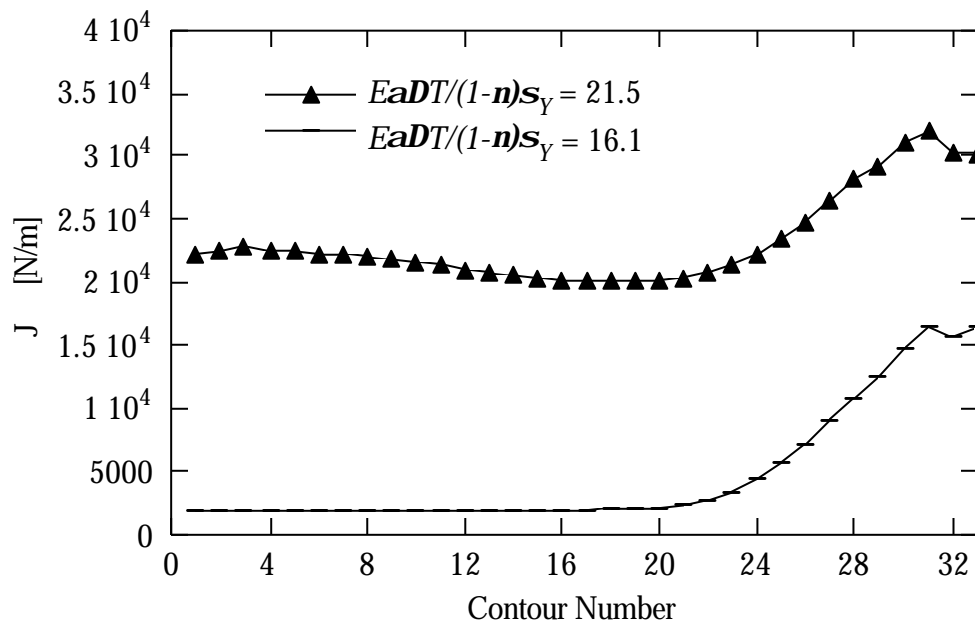
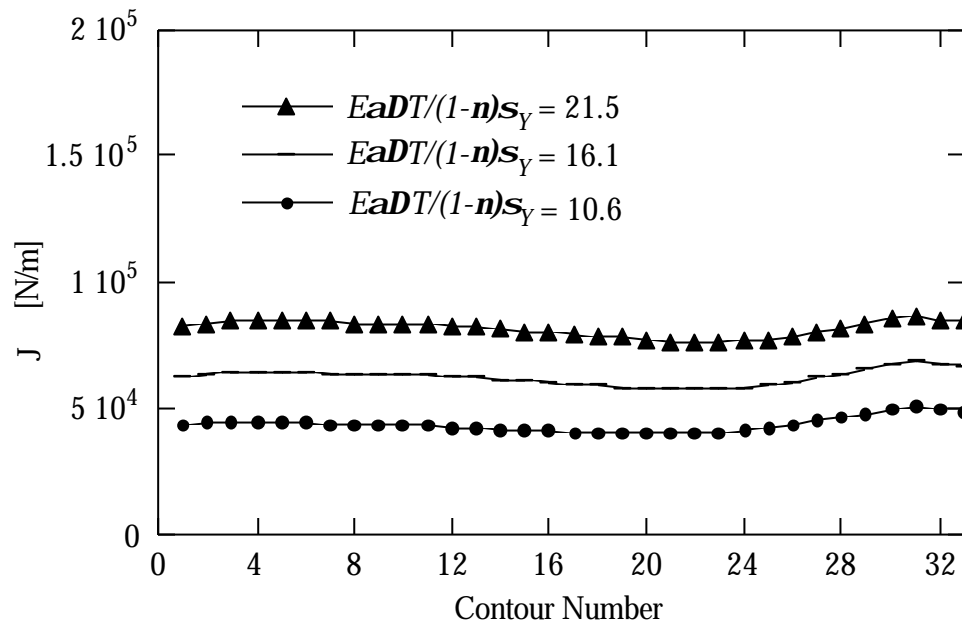


**Figure B4** The  $J$ -integral values for 33 different contours of integration for the welded pipe subjected thermal loading according to equation (5).

### APPENDIX C. CTOD EVALUATION IN POWER LAW MATERIALS

The four noded and the eight noded plane stress elements were compared. The material properties are described by a Ramberg-Osgood material with  $n = 5$ , see figure C2. The geometry modelled was a single edge notched tension SEN(T) panel with  $a/W = 0.5$  and  $W = 7.1$  mm. The maximum load level was about 1.2 times the limit load i.e.  $P_{max} = 1.2 P_g$ . Very small elements were needed to resolve *CTOD* properly. Typically the side of the smallest element  $l_0$  needs to be of the order of a few  $10^{-3}$  mm.

The figures C1-C2 are showing the results of the analysis. Table C1 shows the most interesting results from the two analyses. *CTOD* is evaluated using the undeformed distance from the crack-tip.

**Table C1**

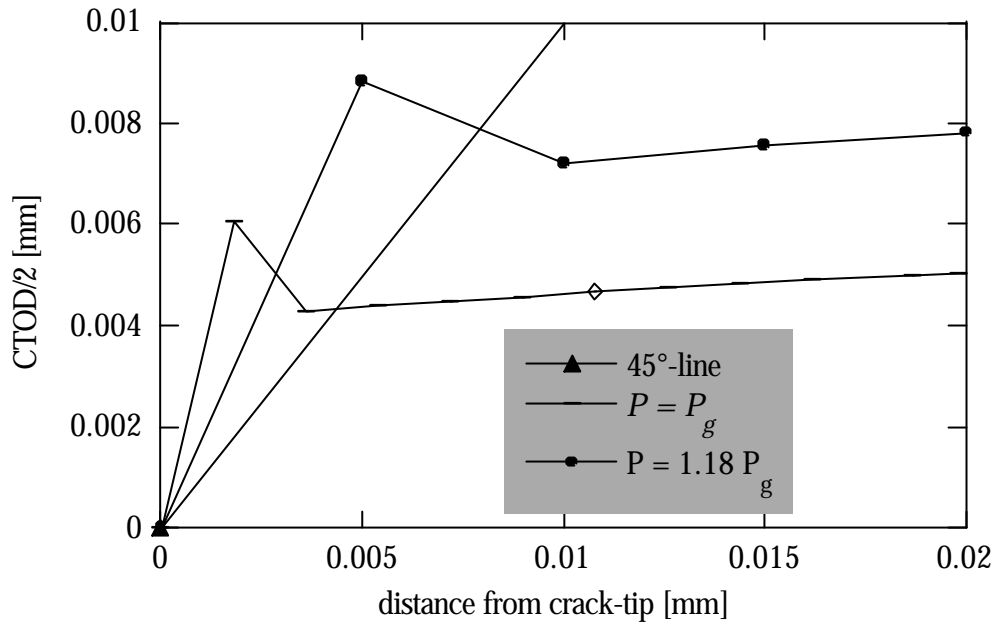
	$P/P_g$	$J$ [kN/m]	$CTOD$ [mm]	$d_n$	$l_0$ [mm]	$\frac{CTOD}{l_0}$
4-noded element	1.0	9.01	0.0070	0.31	0.0018	3.9
	1.18	15.05	0.0124	0.33	0.005	2.5
8-noded element	1.0	8.95	0.0070	0.31	0.003	2.3
	1.23	17.76	0.0140	0.31	0.005	2.8

The non-dimensional-parameter  $d_n$  [14] in the table is determined by

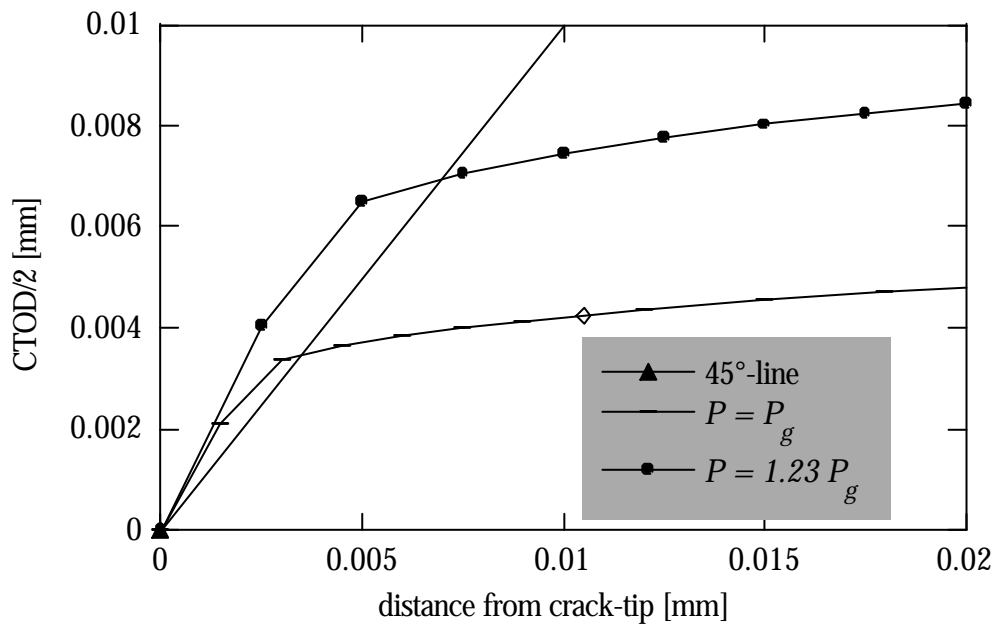
$$CTOD = d_n \frac{J}{\sigma_y} \quad (C1)$$

where  $\sigma_y$  is the uniaxial yield stress. The  $d_n$  values for 8-noded element corresponds better with the HRR value 0.31 for  $n=5$ . Also the convergence of solutions is better for the 8-noded elements.

On the basis of results of this analysis, it was decided to use 8-noded finite elements with an element size close to the crack-tip of a few  $10^{-3}$  mm in order to resolve *CTOD* to a reasonable degree.



a)



b)

**Figure C1** The crack opening profile for SEN(T) with  $a/W = 0.5$  and  $W = 7.1$  mm modelled with  
 a) 4-noded and  
 b) 8-noded plane stress elements.

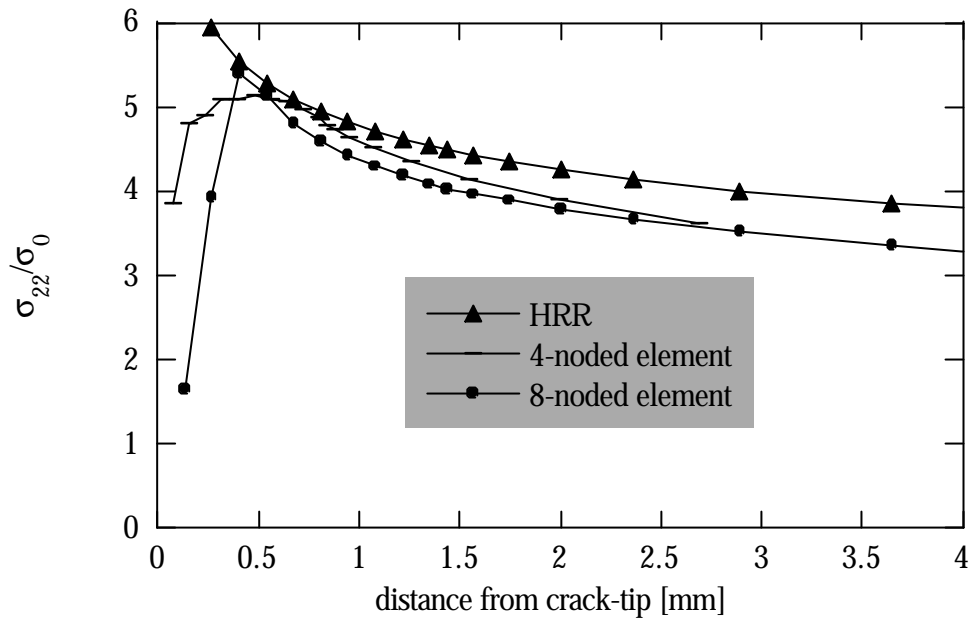
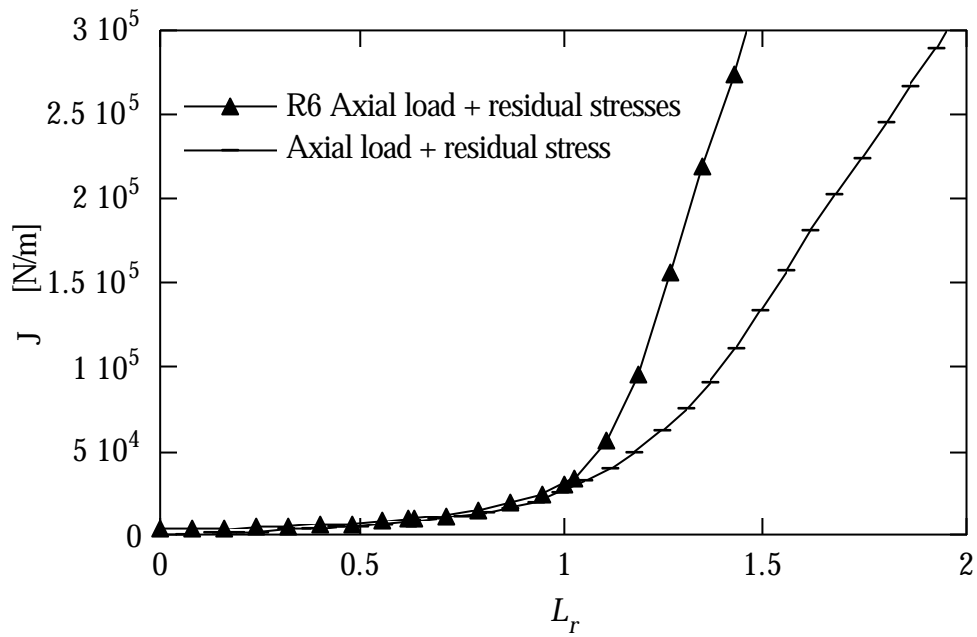


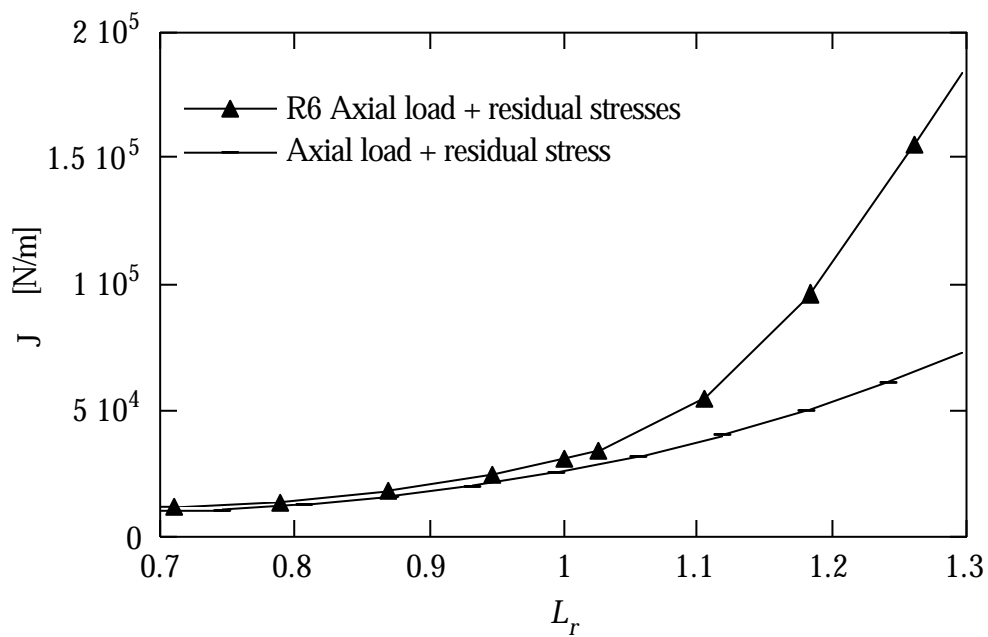
**Figure C2** The HRR field compared with 4-noded and 8-noded elements.

#### APPENDIX D. A HANDBOOK-BASED LIMIT LOAD DEFINITION

The definition of the limit load is to some extent arbitrary. The  $J$ -integral calculated using the R6-method is dependent on this choice. Figure D1 shows the  $J$ -integral as an increasing axial tensile load was applied to the pipe both with and without residual stress present. The limit load is chosen to have a value of 162 MPa. It is seen that in contrast with the result of Chapter 3, where  $P_g = 228$  MPa, the R6-procedure gives conservative results for all values of  $L_r$ . In figure 3, it is shown that at  $P = 162$  MPa the ligament is mainly deformed elastically, which indicates that it does not represent the true plastic collapse solution. The reason for this is that in the limit load solutions used in standard handbooks, such as [4], the limit load is obtained when the axial stresses equals the yield stress  $\sigma_Y$  in the ligament.



a)



b)

**Figure D1.** a) The  $J$ -integral as a function of  $L_r$ .

b)  $J - L_r$  resolved for load values closer to  $L_r = 1.0$ . The  $L_r$ -definition used is based on the handbook solution [4],  $P_g = 162\text{MPa}$ , rather than  $P_g = 228\text{MPa}$ , which is the limit load used in Chapter 3 and Appendix B